



# Hydrological regimes in different slope environments and implications on rainfall thresholds triggering shallow landslides

Francesco Fusco<sup>1,2</sup> · Massimiliano Bordini<sup>3</sup> · Rita Tufano<sup>2</sup> · Valerio Vivaldi<sup>3</sup> · Claudia Meisina<sup>3</sup> · Roberto Valentino<sup>4</sup> · Marco Bittelli<sup>5</sup> · Pantaleone De Vita<sup>2</sup>

Received: 13 April 2021 / Accepted: 22 May 2022 / Published online: 28 June 2022  
© The Author(s) 2022

## Abstract

Assessing hazard of rainfall-induced shallow landslides represents a challenge for the risk management of urbanized areas for which the setting up of early warning systems, based on the reconstruction of reliable rainfall thresholds and rainfall monitoring, is a solution more practicable than the delocalization of settlements and infrastructures. Consequently, the reduction in uncertainties affecting the estimation of rainfall thresholds conditions, leading to the triggering of slope instabilities, is a fundamental task to be tackled. In such a view, coupled soil hydrological monitoring and physics-based modeling approaches are presented for estimating rainfall thresholds in two different geomorphological environments prone to shallow landsliding. Based on the comparison of results achieved for silty-clayey soils characterizing Oltrepò Pavese area (northern Italy) and ash-fall pyroclastic soils mantling slopes of Sarno Mountains ridge (southern Italy), this research advances the understanding of the slope hydrological response in triggering shallow landslides. Among the principal results is the comprehension that, mainly depending on geological and geomorphological settings, geotechnical and hydrological properties of soil coverings have a fundamental control on the timing and intensity of hydrological processes leading to landslide initiation. Moreover, results obtained show how the characteristics of the soil coverings control the slope hydrological response at different time scales, making the antecedent soil hydrological conditions a not negligible factor for estimating landslide rainfall thresholds. The approaches proposed can be conceived as an adaptable tool to assess hazard to initiation of shallow rainfall-induced landslides and to implement early-warning systems from site-specific to distributed (catchment or larger) scales.

**Keywords** Rainfall-induced shallow landslides · Hillslope hydrology · Soil hydrological monitoring · Hydrological modeling · Physics-based rainfall thresholds

---

✉ Rita Tufano  
rita.tufano@unina.it

✉ Valerio Vivaldi  
valerio.vivaldi@unipv.it

## 1 Introduction

In the framework of approaches used to reduce and mitigate risks related to geohazards, the occurrence of sudden rainfall-induced disasters, such as landslides or floods, is largely tackled with the development and application of non-structural approaches based on early warning systems (EWSs). Criteria for setting territorial EWSs related to rainfall-induced landslides are mainly developed for shallow slope instability phenomena involving surficial soil coverings, derived by weathering or allochthonous deposition, with a depth of few meters. This type of landslides, which are more responsive to recognizable rainfall events (Piciullo et al. 2018), often concentrated in time, allows the clearest identification of triggering rainfall events and the study of critical values, or threshold values, leading to slope instability. However, some efforts have been also made to set up effective EWSs, especially at site-specific scale, for deep-seated and slow-moving landslides which can be affected by reactivation stages, caused by intense or prolonged rainfall events. In these cases, rainfall thresholds are determined by a correlation of rainfall amounts with piezometric levels and ground displacements (Vallet et al. 2016; Crosta et al. 2017; Guo et al. 2019).

Rainfall thresholds are generally used as an essential tool to set EWSs for rainfall-induced shallow landslides, because expressing the onset probability based on relationships between two or more rainfall variables, such as rainfall intensity, cumulative amount and duration (White et al. 1992), whose reaching or exceedance of a threshold value represent the triggering conditions for landsliding (Guzzetti et al. 2007; Rossi et al. 2012; Vessia et al. 2014). After the first pioneering work based on this type of approach (Caine 1980), many others have been developed in the following years, forming a distinct branch in the field of the landslide science (De Vita et al. 1998; Segoni et al. 2018). Essentially there are two general methods for reconstructing rainfall threshold: empirical and deterministic, or physics-based.

Empirical approaches allow the estimation of rainfall thresholds through the recognition of cause-effect relationships between past landslide events and associated rainfall records (i.e., Kim et al. 1991; Crosta and Dal Negro 2003; Brunetti et al. 2010; Tien Bui et al. 2013; Segoni et al. 2014a, b; Vennari et al. 2014; Gariano et al. 2015; Rosi et al. 2015; Melillo et al. 2016; Mirus et al. 2018a; Tufano et al. 2019; Kim et al. 2021) by the interpretation of bi-variate correlations (e.g., Caine 1980; Crozier and Eyles 1980; Glade et al. 2000; Guzzetti et al. 2008). At this regard, many attempts were carried out for identifying rainfall thresholds values, based on pure heuristic or statistical criteria. Moreover, empirical thresholds were considered at different scales, from global (Caine 1980; Innes 1983; Jibson 1989; Cannon and Gartner 2005) to regional (e.g., Moser and Hohensinn 1983; Galanti et al. 2018) and local (Wieczorek et al. 2000; Mirus et al. 2018b), depending on the extent of the analysis carried out. Although these empirical approaches are commonly used for rainfall-induced shallow landslides assessment at different scales, different types of uncertainties concerning data and methods considered may strongly affect their reliability, especially if coupled with EWSs. Three main groups of uncertainties can be summarized (Melillo et al. 2018): (i) availability and quality of both rainfall measurements, depending on altimetric and planimetric distances between rain gauge stations and landslide source areas, and completeness of landslide inventories (Tufano et al. 2019); (ii) identification of rainfall sequences causing landslides (Vessia et al. 2014); (iii) heuristic or statistical methods used to define rainfall thresholds. In addition, temporal resolution of rainfall recordings, from minute to daily time scales, controls the extent in duration of empirical rainfall thresholds (Gariano et al. 2020). Besides these types of errors, dynamic factors

predisposing to slope instability, such as antecedent soil hydrological conditions (Rahardjo et al. 2001; Yune et al. 2010; Kim et al. 2013; Bogaard and Greco 2018) and geotechnical aspects of involved soils (De Luca and Versace 2017), represent not negligible sources of uncertainties which can affect severely EWSs by a high number of false positive and negative cases (Nikolopoulos et al. 2014; Peres et al. 2017). Several attempts were made to consider the effects of antecedent rainfall conditions, because intended as predisposing factor to slope instability (Crozier 1986; Wieczorek 1996). Specifically, various methods have been proposed to take into account the combined effect of antecedent soil moisture conditions and rainfall triggering event on the occurrence (or the lack of occurrence) of shallow landslides, using the relationship between daily rainfall features and antecedent cumulative rainfall (Kim et al. 1991; Glade et al. 2000; Dahal and Hasegawa 2008; Rosi et al. 2021). Results of several researches testify the difficulty in defining the optimal antecedent rainfall period (Fuhrmann et al. 2008). Vessia et al. (2014) analyzed a sample of 100 shallow landslides collected in Italy and implemented an automated procedure consisting in a 1-month track of antecedent rainfall during dry and wet seasons, with two possible dry periods of 48 h and 72 h, to automatically reconstruct different rainfall patterns that can trigger shallow landslides.

In pyroclastic soil-mantled slopes of Campania region (southern Italy), significant relationships between daily rainfall and antecedent rainfall cumulative on durations up to 5, 10, 20, 40, and 60 preceding days were found by De Vita and Piscopo (2002), while Rosi et al. (2021) developed three-dimensional rainfall thresholds for the Emilia Romagna region (Northern Italy) based on rainfall intensity and duration with the mean rainfall amount, estimated antecedent periods between 7 and 30 days. This approach allowed obtaining better performances than the traditional intensity–duration thresholds, especially due to a significant reduction in false positive rate (at least of 20%). Other researchers have considered antecedent conditions by different approaches. Glade et al. (2000) considered the Antecedent Soil Water Status (ASWS) model, consisting in a simplified conceptual model that estimates soil moisture on a daily time scale. Godt et al. (2006) proposed an Antecedent Water Index (AWI) based on a water balance and to its combination with a rainfall intensity–duration empirical threshold by a decision tree.

Physics-based (deterministic) approaches, based on coupled hydro-mechanical numerical modeling and slope stability analysis, were proposed by many authors to reduce uncertainties or lack of data affecting empirical rainfall thresholds, (e.g., Terlien 1998; Godt et al. 2008; De Vita et al. 2013, 2018; Peres and Cancelliere 2014; Napolitano et al. 2016; Tufano et al. 2016; Thomas et al. 2018; Bordoni et al. 2019; Marin and Velásquez 2020). Specifically, the deterministic approaches estimate the hydrological response of site-specific geomorphological slope conditions, which are prone to shallow landsliding under a rainfall event (Bordoni et al. 2019), by using detailed hydrological, hydraulic and geotechnical information. Therefore, physics-based models are currently limited to site-specific investigations or hypothesis testing (Thomas et al. 2018). As for the empirical thresholds, the physics-based ones may result in the same criticalities such as missed warnings or false alarms due to inaccuracies of parameters and conditions of slope hydro-mechanical models considered.

To reduce inaccuracies of empirical thresholds, Vessia et al. (2020) introduced a method (MAPs), based on a multivariate geostatistical approach, to take into account both geomorphological and climate data. At the same way, several attempts have also done to reduce inaccuracies of physics-based approach considering the effect of antecedent soil hydrological conditions on the landslide triggering. In this case, rainfall thresholds are considered as non-stationary depending on antecedent soil moisture (Napolitano et al. 2016; De Luca

and Versace 2017). At this regard, many authors (e.g., Collins and Znidarcic 2004; Sidle and Ochiai 2006; Lu and Godt 2013; Bogaard and Greco 2016) have demonstrated that the increase in antecedent soil pore-water pressures head, even in unsaturated conditions, leads to a decrease in soil shear strength, thus behaving as a predisposing condition to the slope failure under a given rainfall event. Contrarily, the decrease in antecedent soil water pressure head hampers the possibility of slope instability under the same rainfall condition.

Besides the studies needed for setting up the physical model of a slope, including detailed morphological, lithological, geotechnical and hydrological characterizations of potentially unstable soil horizons, in recent years field soil hydrological monitoring has become progressively a fundamental achievement to assess slope hydrologic response and to calibrate the hydrological numerical modeling (Greco et al. 2013; Lu and Godt 2013; Comegna et al. 2016; Fusco et al. 2017, 2019; Bordoni et al. 2019).

Considering the relevance of slope hydrological response in defining physics-based rainfall thresholds and its dependence on local geological, hydrogeological and climatic factors, in this paper the comparison of studies carried out in two distinct geomorphological environments with a high proneness to shallow landsliding is proposed: the clayey hilly area of Oltrepò Pavese (Lombardy region—northern Italy) and the ash-fall pyroclastic soil mantled mountain slopes surrounding the Somma-Vesuvius volcano (Campania region—southern Italy).

Due to the strong differences in geological, geotechnical, hydraulic characteristics and soil hydrological response, recognized by field soil hydrological monitoring, the comparison was intended useful to understand the effects of different slope hydrological responses on the estimation of physics-based rainfall thresholds and, therefore, its implications in supporting EWSs at site-specific scale. Results obtained are expected as being exportable at the catchment or wider scales depending on the representativeness of the selected test-sites of geological, geomorphological and hydrological conditions of the whole area.

## 2 Comparison of study areas

### 2.1 Climate

#### 2.1.1 Montuè test site (Ms)

Located in the physiographic unit of the northern Apennines, along the south-western border of the Po' Plain, the test site of Montuè ( $M_S$ ) (170–210 m a.s.l.) coincides with the hilly north-eastern Oltrepò Pavese area, within the Rio Frate catchment, about 10 km south of Pavia city (Lombardy region, northern Italy; Fig. 1). According to Köppen (1936) climate classification (Geiger 1954), the test site is characterized by a temperate-mesothermal climate. Meteorological data recorded by the Canevino weather station (455 m a.s.l.), managed by the Regional Agency for Environmental Protection (Station ID# 9108), from January 2004 through October 2020, show that climate regime in  $M_S$  is sub-continental temperate, as typical of the Po' Plain and Apennine region. Representative climate parameters are indicated by a mean annual temperature of 12.0 °C, with January and July as the coldest (mean value 3.3 °C) and warmest (mean value 24.6 °C) months of the year, respectively. The rainfall regime is characterized by a total mean annual amount of 680.7 mm, with November resulting as the rainiest month (96.2 mm) and July as the driest one (38.7 mm).

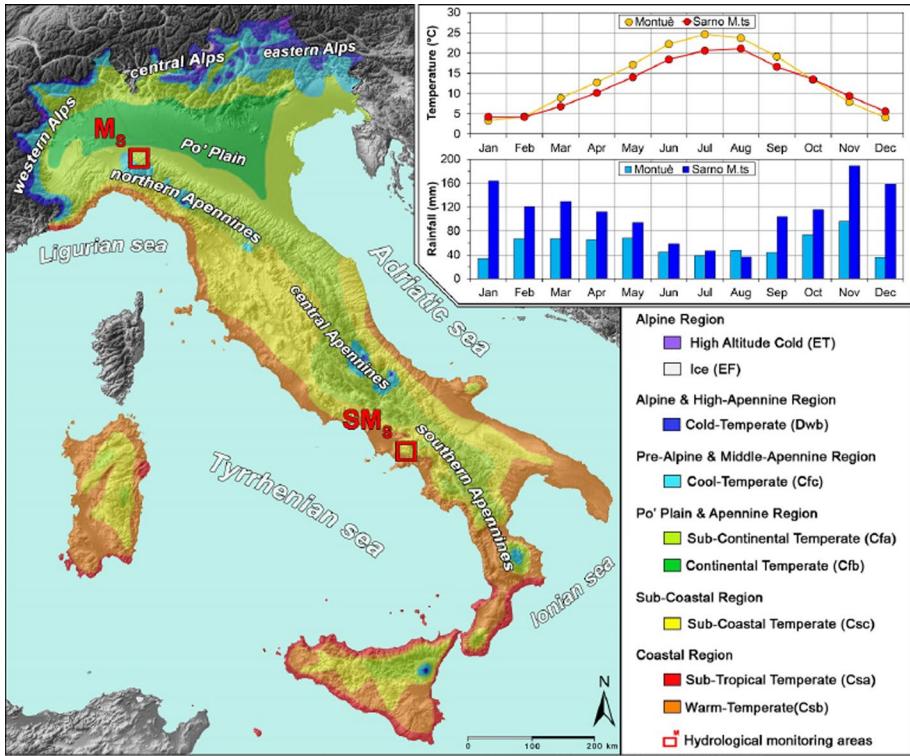


**Fig. 1** Climate classification of Italy (Koppen-Geiger 1954) with indication of Montuè (Ms) and Sarno Mountains (SMs) test sites. Climate data including mean monthly values of air temperature and rainfall are shown (Canevino meteorological station managed by Regional Agency Environmental Protection ID# 9108,) for M<sub>S</sub> site; Torriello meteorological station managed by the Civil Protection Department ID# 15285, for SM<sub>S</sub> site

### 2.1.2 Sarno Mountains test site (SMs)

The test site of Sarno Mountains (SM<sub>S</sub>) (about 925 m a.s.l.), is located along the south-western slope of Mount Pizzo D’Alvano (1.133 m a.s.l.), the highest peak of this mountains range (Campania region, southern Italy; Fig. 1). This area belongs to a sector of the southern Apennines coinciding with the northeast border of the Campanian Plain, about 20 km west from the Somma-Vesuvius volcano. SM<sub>S</sub> is characterized by a typical Mediterranean climate (sub-coastal region), with humid winters and hot summers. Considering meteorological recordings of Torriello weather station (840 m s.l.m.), managed by the Civil Protection Department (Station ID# 15285) and active since May 1998, the mean annual temperature value is 12.1 °C. The coldest month coincides with February (mean value 4.1 °C) while August represents the warmest one (mean value 21.0 °C). The mean annual amount of rainfall is 1303.1 mm with November as the rainiest month (188.9 mm), the rainy period lasting until January (~40% of total annual rainfall amount), and July as the least rainy month (36.5 mm).

**Fig. 2 a** Geological setting of the Oltrepò Pavese area comprising the Montuè (Ms) test site: (1) alluvial deposits; (2) Miocene sandstones (Monte Arzolo Sandstones); (3) Miocene conglomerates (Rocca Ticozzi Conglomerates); (4) Miocene marls and sandy marls (Sant'Agata Fossili Marls); (5) Miocene gypsum (Gessoso-Solfifera Formation); (6) outcropping and buried faults. **b** Geological setting of the peri-Vesuvian area comprising the Sarno Mountains (SMs) test site: (1) alluvial deposits; (2) travertine deposits; (3) debris and slope talus deposits; (4) incoherent ash-fall deposits (Recent Pyroclastic Complex); (5) mainly coherent ash-fall deposits (Ancient Pyroclastic Complex); (6) lavas; (7) Miocene flysch; (8) Middle Jurassic–Upper Cretaceous limestones; (9) Lower Triassic–Middle Jurassic dolomites and calcareous limestones; (10) outcropping and buried faults; (11) total isopachs line (in m) of ash-fall pyroclastic deposits erupted by the Plinian Somma-Vesuvius's eruptions (modified from: De Vita et al. 2006, De Vita and Nappi 2013); (12) study areas

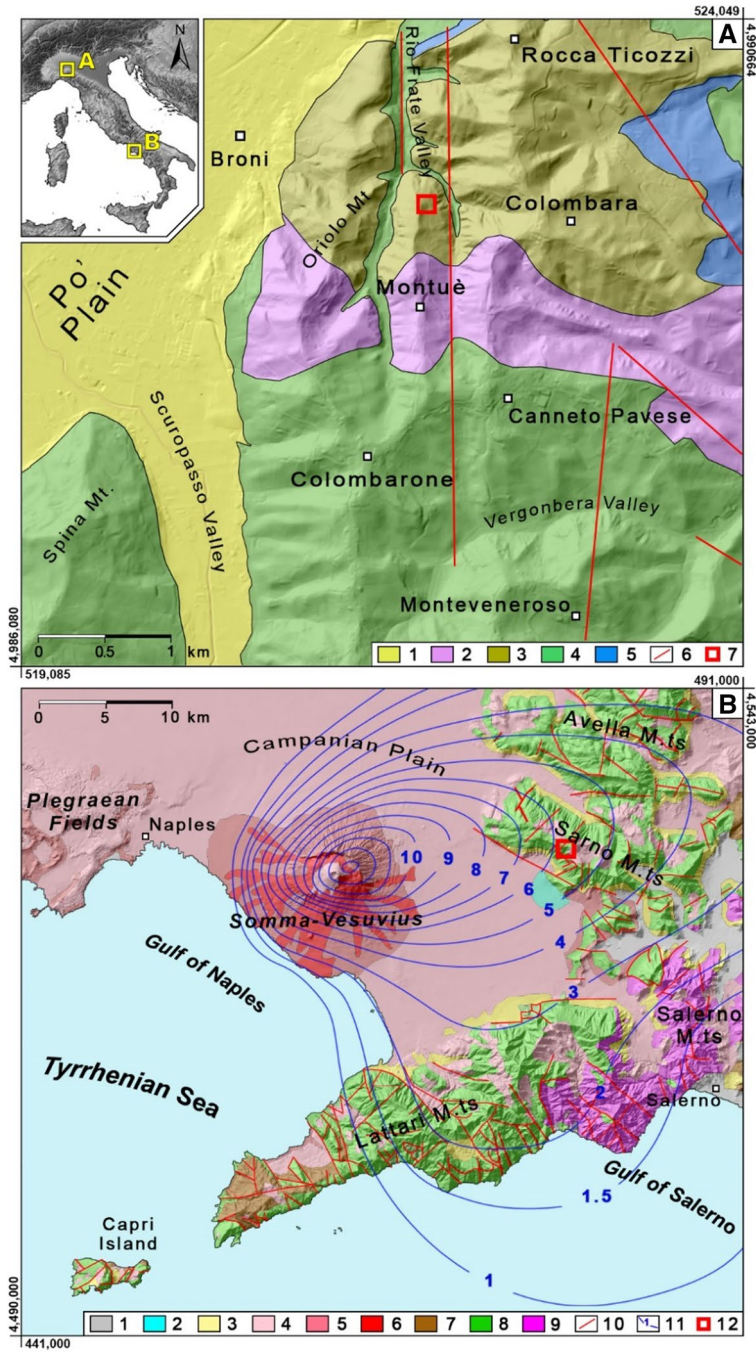
## 2.2 Geology and pedology

Different geological features characterize the two test sites, whose lithostratigraphic settings are strongly related to pre- and syn-orogenic phases of the Apennines chain formation. Moreover, such test-sites were considered as representative of the main geological, pedological, hydrological and geomorphological features of the investigated area.

### 2.2.1 Montuè test site (Ms)

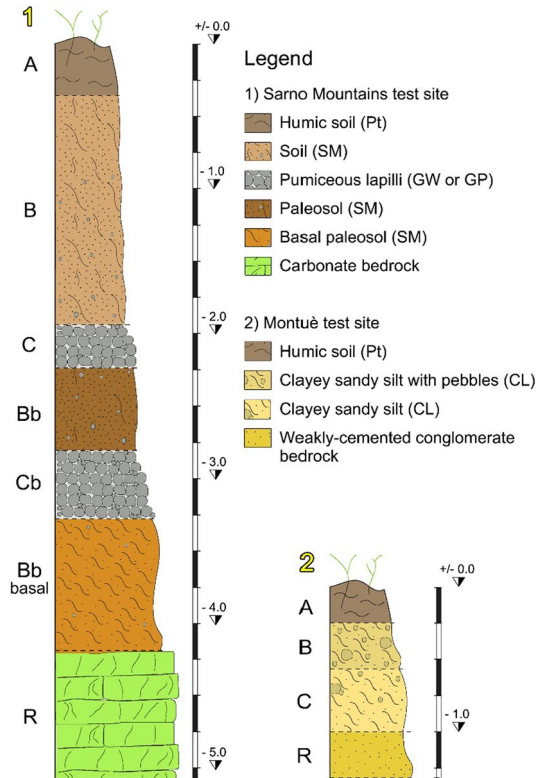
The sector of Oltrepò Pavese, to which the  $M_S$  test site belongs, is characterized by the *Margine* Miocene-Pliocene series (Vercesi and Scagni 1984), mainly east-northeast dipping with very low dip angle, which is in tectonic contact with Cretaceous turbidite deposits formed by medium-to-thinly bedded or massive limestones (Toscani et al. 2006). The bedrock of  $M_S$  test site is constituted by continental deposits of sands, sandstones and conglomerates (*Monte Arzolo Sandstones* and *Rocca Ticozzi Conglomerates*) overlying marine marls and evaporitic chalks (*Sant'Agata Fossili Marls* and *Gessoso-Solfifera Formation*) (Fig. 2a). In particular, in the  $M_S$  test site the bedrock comprises gravels, sands and weakly-cemented conglomerates with a limited amount of marls (*Rocca Ticozzi Conglomerates*). Eluvial and colluvial deposits (regolith zone), resulting from weathering of bedrock, cover the Miocene–Pliocene succession with variable thickness, varying from few centimeters up to 2.5 m (Zizioli et al. 2013).

Field observations and laboratory geotechnical and hydraulic tests allowed to characterize stratigraphic setting and classify soil horizons by Unified Soil Classification System (ASTM D2487-11) and pedological (USDA 2014) classifications. In detail, soils covering  $M_S$  test site and the surrounding areas, are constituted by Calcic Gleysol soils according to IUSS Working Group WRB (2014), up to 2.5 m thick (Bordoni et al. 2015). Soil profile corresponds to a weathering profile (regolith) of weakly-cemented conglomerates (bedrock), belonging to Miocene-Pliocene deposits of the Oltrepò Pavese area (Figs. 2a, 3). The relevant presence of carbonates as soft coating (> 15%) and gleyic properties into soils are justified by the occurrence of temporary saturated conditions leading to a reducing geochemical environment. The representative stratigraphic setting of soil cover in the  $M_S$  test site is constituted by (Bordoni et al. 2015; Fig. 3): (1) A soil horizon, consisting of organic-rich (Pt) porous and dark-brown clayey sandy silt (CL) with a shallower level characterized by soft carbonate concretions and plant remains (OL); (2) B soil horizons, constituted of porous and brown clayey sandy silt with pebbles (CL) and diffuse presence of carbonate concretions; (3) C soil horizon, formed by compact and brown clayey sandy silt (CL) with



thin (up to 0.2 m) and discontinue calcic horizon enriched in harder carbonate concretions; (4) R horizon, coinciding with weakly-cemented conglomerates bedrock. Grainsize curves of soil horizons (Fig. 4a) and USDA classification (Fig. 4c) showed a predominantly silty

**Fig. 3** Representative stratigraphic setting of soil covers mantling: Sarno Mountains (SMs) (1) and Montuè (Ms) (2) test sites. Soil horizons were indicated following pedological (USDA 2014), lithological and engineering soil classification (USCS)



component with both high content of clay and low percentages of sand and gravel. According to USCS classification, soil horizons in the  $M_S$  test site are mainly low-plastic or low plastic soils (CL), which can pass to medium plastic or high plastic soils (CH) due to local heterogeneities (Fig. 4d). Similar dry unit weight ( $\gamma_d$ ) and void index ( $e$ ) values characterize the soil horizons (Table 1; Fig. 5).

## 2.2.2 Sarno Mountains test site (SMs)

The  $SM_S$  test site coincides with the Sarno Mountains ridge, a mountain range belonging to the arc-shaped mountainous zone surrounding the Phlegraean Fields and Somma-Vesuvius volcanic centers of the Campania region (Fig. 2b). These mountain ranges are constituted of Mesozoic carbonate platform series, which were shaped by the Pliocene and Pleistocene tectonic phases forming presently steep structural slopes (Patacca and Scandone 2007; Vitale and Ciarcia 2018). During the late Quaternary, until historical times, these slopes were covered by ash-fall pyroclastic deposits, mainly erupted by the closer and younger Somma-Vesuvius volcano (Recent Pyroclastic Complex; RPC) and subordinately by the Phlegraean Fields volcanoes (Ancient Pyroclastic Complex; APC). Empirical analyses showed a good matching between observed thicknesses (De Vita et al. 2006; Vita and Nappi 2013; Del Soldato et al. 2018) and those theoretically expected by isopach maps derived by the volcanological literature (Fig. 2b), with maximum values varying from 7.0 to 4.0 m in the slope angle range lower than  $28^\circ$ . Instead, an inverse relationship between



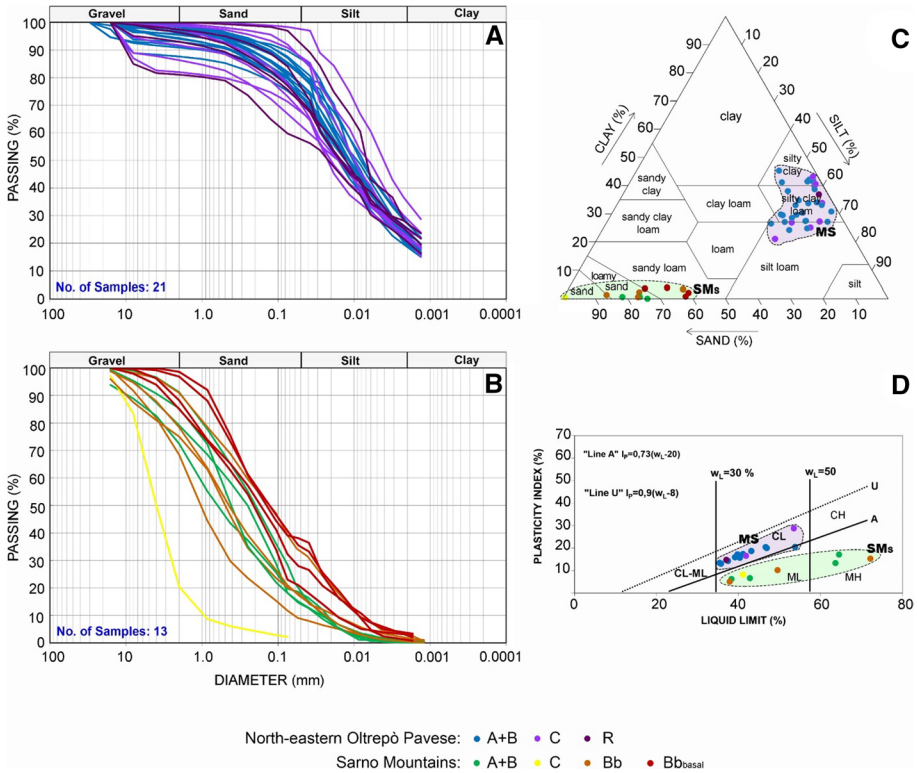


**Fig. 4** Grain size curves for soil horizons of north-eastern Montuè (Ms) (a) and Sarno Mountains (SM<sub>s</sub>) (b) test sites. Pedological (c; USDA 2014), lithological and engineering soil classification (d; USCS) were also shown. The number of soil samples considered is indicated

**Table 1** Mean values of hydro-mechanical parameters for Montuè (Ms) and Sarno Mountains (SMs) test sites

Test Site	Soil Horizon	$K_{sat}$ (m/s)	$\theta_s$ ( $m^3/m^3$ )	$\theta_r$ ( $m^3/m^3$ )	$A$ (ad)	$n$ (ad)	$\gamma_d$ ( $kN/m^3$ )	$\varphi'$ (°)	$c'$ (kPa)
Montuè	A	$1.00 \times 10^{-5}$	0.330	0.023	0.004	1.55	14.9	26	3.5
	B	$1.80 \times 10^{-5}$	0.400	0.021	0.012	1.38	15.1	28	0.0
	C	$8.00 \times 10^{-7}$	0.440	0.072	0.010	1.21	15.0	26	29.0
Sarno Mountains	A + B	$8.71 \times 10^{-5}$	0.500	0.080	5.600	1.57	10.22	32	4.5
	C	$7.71 \times 10^{-3}$	0.560	0.001	4.200	1.43	8.42	37	0.0
	Bb	$1.62 \times 10^{-5}$	0.590	0.200	0.730	1.32	10.33	34	1.8
	B <sub>basal</sub>	$3.54 \times 10^{-6}$	0.630	0.110	7.200	1.11	6.83	35	8.1

Key to symbols:  $K_{sat}$ , saturated hydraulic conductivity;  $\theta_s$ , saturated volumetric water content;  $\theta_r$ , residual volumetric water content;  $\alpha$  and  $n$ , fitting parameters;  $\gamma_d$ , dry weight unit;  $\varphi'$ , effective friction angle;  $c'$ , effective cohesion

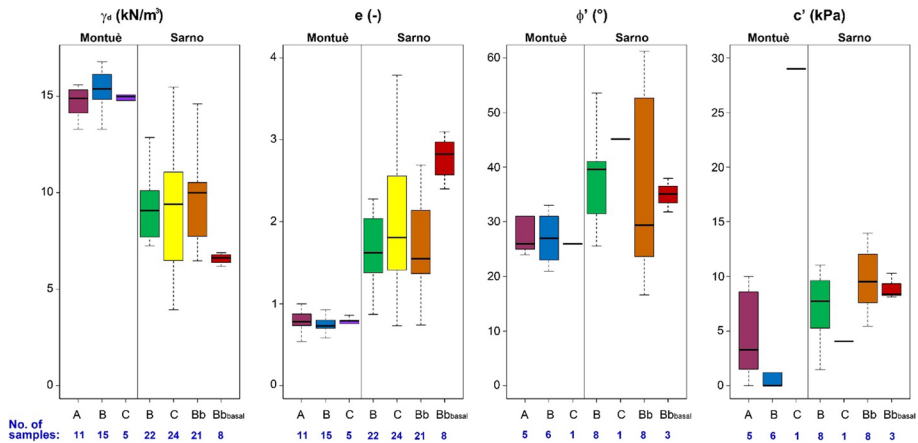


**Fig. 5** Main geotechnical parameters of soil horizons characterizing Montuè (Ms) and Sarno Mountains (SMs) test sites. Key to symbols:  $\gamma_d$  = dry unit weight;  $e$  = void index;  $\phi'$  = effective friction angle;  $c'$  = effective cohesion. The number of soil samples considered is indicated

thickness of the ash-fall pyroclastic mantle and slope angle for values between  $28^\circ$  and  $50^\circ$  was found, with negligible or null values for steeper conditions.

The  $SM_S$  test site is characterized by steep slopes formed by a Mesozoic carbonate bedrock which are mantled by ash-fall pyroclastic deposits (Figs. 2b, 3). Spatial distribution and thickness of pyroclastic soils is strongly controlled by both local morphological conditions and slope denudational processes (De Vita et al. 2006; Vita and Nappi 2013; Del Soldato et al. 2018).

The representative stratigraphic setting can be summarized as (De Vita et al. 2006; Fig. 3): A soil horizon, characterized by a granular and very porous structure and consisting of abundant roots and organic material (Pt); B soil horizon, formed by highly pedogenized coarse and fine ashes (SM) with a dark from brown-yellowish to brown color and high value of water retention, mainly due to a very porous structure; this soil horizon is classified as Andosol (Terribile et al. 2000); (3) C soil horizon, generally corresponding to deposits of a specific eruption of the Somma-Vesuvius volcano, is constituted of cohesionless pumiceous pyroclasts, weakly weathered (GW or GP); (4) Bb soil horizon, corresponding to a B soil horizon buried by a successive depositional event and thus considerable as a paleosol (SM); (5) Cb soil horizon, representative of a buried C soil horizon (GW or GP); (6) Bb<sub>basal</sub> soil horizon, corresponding to a residual basal pyroclastic deposit, highly weathered by pedogenesis (SM); (7) R horizon, fractured carbonate bedrock with open joints filled in the first few meters by the overlying paleosol. Soil horizons show a significant variability in terms of grain size (Fig. 4b). The negligible presence of clay fraction (Fig. 4c) and low plasticity index confirms a behavior from non-plastic to low plastic (ML and MH) (Fig. 4d). Values of  $\gamma_d$  and  $e$  are, respectively, much lower and higher in comparison with other soil types (Table 1; Fig. 5).

### 2.3 Soil hydraulic and mechanical properties

Mechanical and unsaturated/saturated soil properties deriving from in situ measurements and laboratory tests carried out during previous researches, for both the  $M_S$  (Zizioli et al.

2013; Bordoni et al. 2015) and  $SM_S$  test sites (De Vita et al. 2013), were analyzed comparatively in this study.

### 2.3.1 Montuè test site (Ms)

The effective friction angle ( $\phi'$ ) was determined for the soil cover profile in the  $M_S$  test site (Fig. 5) showing similar values for the shallower soil horizons (A and B), varying between  $20^\circ$  and  $33^\circ$ , while  $26^\circ$  for the deepest one (C) (Table 1). Furthermore, similar values of effective cohesion ( $c'$ ) were found characterizing the A and B soil horizons, ranging between 0 and 10 kPa, while the C soil horizon was recognized as characterized by a higher effective cohesion ( $c'$ ), up to 29 kPa. Concerning the hydraulic soil properties, results testify a general decrease in  $K_{sat}$  values with depth (Bordoni et al. 2019), varying from  $1.0 \times 10^{-5}$  m/s for the shallower A and B soil horizons, down to  $8.0 \times 10^{-7}$  m/s for the deepest ones (C soil horizon) (Table 1). Moreover, these soil horizons are characterized by a significant water retention capacity (Bordoni et al. 2015), especially at high values of matric potential, as typical of clayey/silty soils. Consequently, a high water-retention capacity characterizes soils of the  $M_S$  test site up to about 2.0 m of soil water potential ( $-2.0$  m soil water pressure head), above which a gradual release of intra-granular capillary water occurs. The interpolation of laboratory water retention data by the van Genuchten's Equation (1980) allowed the estimation of Soil Water Retention Curves (SWRCs) (Fig. 6a). SWRCs determined for soil horizons are characterized by similar shapes and ranges, thus confirming similar retention characteristics along the depth, as testified by the narrow ranges of saturated water content ( $\theta_S$ ) ( $0.330$ – $0.440$   $m^3/m^3$ ) and residual water content ( $\theta_R$ ) ( $0.021$ – $0.072$   $m^3/m^3$ ) (Table 1).

### 2.3.2 Sarno Mountains test site (SMs)

Effective friction angle ( $\phi'$ ) resulted with a high variability for the  $SM_S$  test site for which B and Bb soil horizons showed the widest ranges ( $25^\circ$ – $53^\circ$  and  $16^\circ$ – $61^\circ$ , respectively) if compared with the  $Bb_{basal}$  ( $32^\circ$ – $38^\circ$ ) and C ( $45^\circ$ ) soil horizons (Fig. 5; Table 1). This high variability affecting the shallower B and Bb soil horizons is due to the occurrence of coarse lapilli pumiceous pyroclasts, which determined crushing and dilatancy phenomena during direct shear tests (Mitchell and Soga 2005). Furthermore, very few values were considered reliable for the C soil horizons due to the high difficulty in executing direct shear tests on very coarse soils (lapilli, namely gravel). A general low effective cohesion ( $c'$ ) was found for these soil horizons, with quite similar values characterizing pedogenized soil horizons (A + B, Bb and  $Bb_{basal}$ ), ranging between 5.0 and 12.0 kPa, which has been related to both reinforcement of root apparatuses and effect of crushing of lapilli pumiceous pyroclasts. Saturated hydraulic conductivity ( $K_{sat}$ ) values for soil horizons of the  $SM_S$  test site show a strong contrast due to alternating pedogenized soil horizons (Bb and  $Bb_{basal}$ ) (De Vita et al. 2013), with the lowest values ( $8.71 \times 10^{-5}$  m/s  $\leq K_{sat} \leq 3.54 \times 10^{-6}$  m/s), and unweathered pumiceous lapilli of C soil horizon, with the highest values ( $K_{sat}$  up to  $7.71 \times 10^{-3}$  m/s). However, a general decrease in  $K_{sat}$  with depth was recognized if considering the pedogenized soil horizons only. Analyzing parameters of the van Genuchten's Equation (1980) and observing the related SWRCs (Fig. 6), soil horizons show similar  $\theta_S$  values, varying from 0.500 to 0.630  $m^3/m^3$  (Table 1), while different for  $\theta_R$  (Fig. 6b). The latter was found ranging between 0.08  $m^3/m^3$  and 0.20  $m^3/m^3$  for Bb and  $Bb_{basal}$  soil horizons and around 0.001  $m^3/m^3$  for C and Cb pumiceous lapilli soil horizons. Regarding soils

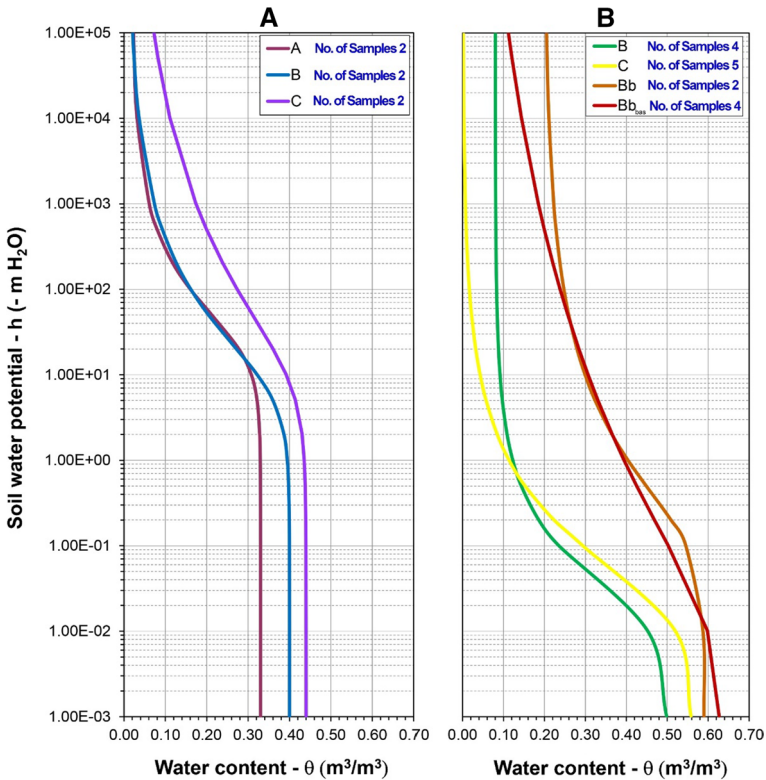


**Fig. 6** Soil water retention curves (SWRCs) obtained by laboratory tests carried out considering soil horizons samples of **a** Montuè (Ms) and **b** Sarno Mountains (SMs) test sites. The number of soil samples considered is indicated

of the SM<sub>5</sub> test site, the gradual release of intra-granular capillary water occurs for soil water potential values higher than 0.01 m (Fig. 6b).

## 2.4 Landslide features

### 2.4.1 Montuè test site (Ms)

Shallow landslides affecting the Oltrepò Pavese and Sarno Mountains areas are typically triggered by intense and/or prolonged rainfall events (Bordoni et al. 2015), particularly if preceded by significant rainy periods, and are characterized by a complex style (*sensu* Cruden and Varnes 1996). More than 1600 shallow landslides affected about 240 km<sup>2</sup> (29 landslides per km<sup>2</sup>) of slopes surrounding M<sub>5</sub> test site, among them the main was that occurred on April, 27th–28th 2009 (160 mm in 62 h; Zizioli et al. 2013). Mentioning further events occurred in the area: (a) between March and April 2013 (227.8 mm in 2 months; Zizioli et al. 2014); (b) between 28th February and 2nd March 2014 (68.9 mm in 42 h, with 105.5 mm in 30 days; Bordoni et al. 2015); (c) between 21st and 22nd December 2019 (31.9 mm in 48 h, with 136.1 mm in 30 days); (d) between 5 and 6th December 2020 (95 mm in 60 h, with 59 mm in the previous 4 days; Bordoni et al. 2021). Specifically, in

Ms test site, several rainfall-induced shallow landslides occurred during April 2009 event and 28th February–2nd March 2014 event, the latter started about 15 m downhill the monitored area.

This type of landslides is characterized by two main evolutionary stages series: (1) soil slips (Campbell 1975) or disintegrating soil slips, where the accumulation zone is not recognizable, with mechanisms of shallow rotational/translational failures (Howard et al. 1988); (2) flow-like mass movements, from rapid to very rapid, with earth flow mechanisms (Hungr et al. 2001, 2014). Usually, they involve soil mantle covering the weathered or un-weathered bedrock with sliding surface located at depths between 0.5 and 2.0 m, coinciding with the contact between the B horizon and C soil horizons or with the bedrock interface (Bordoni et al. 2015, 2021). Involved volumes were assessed varying from 100 to 35,000 m<sup>3</sup>. Source areas are usually located uphill of steep slopes (> 15°), close to abrupt slope angle variations or morphological jugs. Generally, their total length ranges between 10 and 500 m while the width between 10 and 70 m, with a ratio between length and width varying between 1.0 and 7.1. Runout and accumulation zones can affect slopes of limited length (less than 200 m) or portions of longer ones.

#### 2.4.2 Sarno Mountains test site (SMs)

In the Sarno Mountains area (SMs test site) the rainfall induced very-to-extremely rapid debris flows involving ash-fall pyroclastic soils are a well-known national geohazard (Guadagno et al. 2011). The high societal impact of these landslides has made it urgent to research susceptibility to their onset, volumes potentially involved, run-out and triggering-rainfall conditions, especially after the last high-magnitude catastrophic event of 5th and 6th May 1998, which caused the loss of 160 lives (Calcaterra et al. 1999). Unfortunately, the rainfall event was recorded only partially by rain gauges located at the foot-slope of Sarno Mountains, thus with altimetric difference up to 700 m. In the last century, many other deadly rainfall-induced debris flow events involving ash-fall pyroclastic soils occurred in other sectors of carbonate mountain ranges surrounding the Somma-Vesuvius volcano. Among these, the most relevant and deadliest hit Cetara (Amalfi coast) on the 23rd and 24th October 1910, causing 111 victims, and Salerno-Amalfi coast between the 25th and 26th October 1954 causing 316 victims (Esposito et al. 2004).

Also in this case, these shallow landslides are characterized by a complex style (*sensu* Cruden and Varnes 1996). Up to three consecutive evolutionary stages can be identified (Fiorillo et al. 2001; Guadagno et al. 2005; De Vita et al. 2013): (1) initial soil slips (Campbell 1975) or debris slides (Cruden and Varnes 1996) involving from 10<sup>1</sup> to 10<sup>2</sup> m<sup>3</sup> of cubic meters of ash-fall pyroclastic soils (debris, with more than 20% of gravel); (2) debris avalanches (Hungr et al. 2001), involving progressively greater volumes of pyroclastic deposits along open slopes by a dynamic liquefaction mechanism; (3) debris flows (Hungr et al. 2001), characterized by the channeling into the hydrographic network of rapid to very rapid flow-like debris masses. Therefore, debris flows can be defined “landslide-triggered debris flow” (Jakob and Hungr 2005) due to constant occurrence of an initial debris slide-soil slip. However, in some cases, depending on local morphological and soil thickness conditions, debris slides-soil slips can develop into an avalanche only (debris avalanche) and not evolving in a debris flow, thus stopping their movement along the slope or at the footslope.

Interestingly, throughout the source areas of initial debris slides, the Bb<sub>basal</sub> soil horizon was always observed outcropping, thus demonstrating the formation of the initial surface of rupture within the ash-fall pyroclastic soil mantle. Over recent years, some authors

identified the basic factors controlling the susceptibility to initial landsliding, which were recognized in small-scale specific geomorphological and anthropogenic features, such as knickpoints, morphological discontinuities related to outcropping carbonate rocky cliffs and artificial cuts into the pyroclastic mantle, excavated for the construction of mountain roads (Di Crescenzo and Santo 2005; Guadagno et al. 2005; De Vita et al. 2013). The triggering mechanism of the initial slides was related to an unsaturated/saturated throughflow process occurring within the ash-fall pyroclastic soil mantle itself (De Vita et al. 2013) during heavy rainstorms.

### 3 Data and methods

#### 3.1 Soil hydrological monitoring

To assess slope hydrological processes within the soil cover, and variability of soil hydrological response, from hourly to seasonal time scales, field soil hydrological monitoring stations were set up in both test sites (Fig. 7).

##### 3.1.1 Montuè test site (Ms)

Regarding the  $M_s$  test site, a coupled meteorological and soil hydrological monitoring station was installed upslope of one of the triggering areas of the 27th–28th April 2009 landslide event (Fig. 7a). The monitoring site is characterized by a regular planar slope profile, with slope angle varying from  $26^\circ$  to  $35^\circ$ . The slope is eastward oriented and located

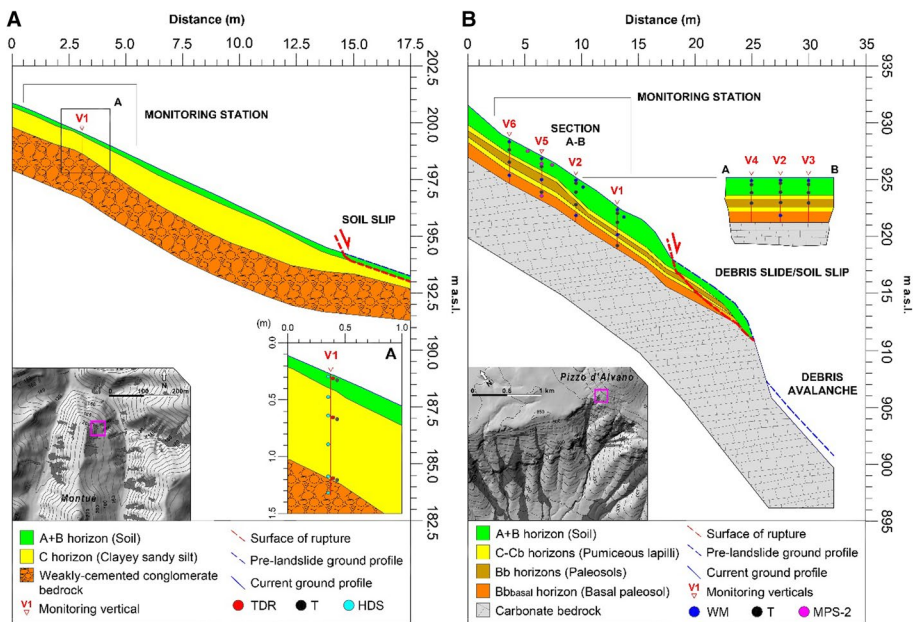


**Fig. 7** Geological models of Montuè (Ms) (a) and Sarno Mountains (SMs) (b) test sites. Locations of monitoring verticals and sensors type are also showed

at medium–low elevation (170–210 m a.s.l.). Shrubs and woodlands of black robust trees (*Robinia Pseudoacacia*) characterize the vegetation type of the area. Trench pits and micro-boreholes carried out in the area allowed the assessment of soil thickness (Bordoni et al. 2015), ranging from few tens of centimeters at slope top to about 1.5 m downslope of the monitoring station. The representative soil profile found at the site of the monitoring station is that described in the previous sections (par. 2.2). The soil hydrological monitoring station was designed to assess seasonal variation of soil water content and soil pore-water pressure head (PH) at different depths range along an instrumented vertical (Bordoni et al. 2015; Table 2). Sensors were installed in the upslope wall of a trench pit allowing the monitoring in natural and undisturbed conditions. Monitoring sensors consist of six Time Domain Reflectometer (TDR) probes (Campbell Scientific, Inc.), equipped with a multiplexer (Campbell Scientific, Inc.) and three tensiometers (Soil moisture, Inc.), installed in each soil horizons. Furthermore, three Heat Dissipation (HD) sensors (Campbell Scientific, Inc.) were installed to extend measurement range. Meteorological and soil sensors were cabled and connected to a datalogger (Campbell Scientific, Inc.) with 10 min acquisition time. Finally, a weather station consisting in a rain gauge (Young Comp.), a barometer (Campbell Scientific, Inc.), a thermo-hygrometer (Campbell Scientific, Inc.), a net radiometer (Kipp & Zonen) and an anemometer (Campbell Scientific, Inc.) were installed.

### 3.1.2 Sarno Mountains test site (SMs)

Hydrological monitoring station for the SM<sub>s</sub> test site is located along the southwestern sector of Mount Pizzo D’Alvano (Fig. 7b), upslope one of the source areas of May 1998 landslides, in the altitude range from 915 to 930 m a.s.l. A fairly regular and steep profile characterizes the monitoring area, with average slope angle of about 35° down to the landslide scarp which is followed downslope by a slope morphological discontinuity corresponding to a rocky scarp, about 5.0 m height, in which the carbonate bedrock outcrops. Consequently, exploratory pits and light dynamic penetration tests (DPLs) as well as topographic surveys allowed the reconstruction of a detailed engineering geological model across the source area (Fusco et al. 2013; Fusco and De Vita 2015), which is consistent

**Table 2** Type and number of sensors installed for soil PH monitoring at different depth zones in Montuè (Ms) and Sarno Mountains (SMs) (except for the C horizon) test sites

Test Site	Soil Horizon	Sensor type			N° of sensors	Range Depth (m)
		T	TDR	HDS		
Montuè	A	1	1	1	3	0.0 ÷ 0.2
	B	1	3	1	5	0.4 ÷ 1.0
	C	1	2	1	4	1.2 ÷ 1.4
		T	WM	MPS-2		
Sarno Mountains	B	16	8	3	27	0.0 ÷ 1.5
	Bb	5	2	1	8	1.8 ÷ 2.5
	Bb <sub>basal</sub>	2	2	1	5	3.5 ÷ 4.0

Key to symbols: T, Tensiometer; TDR, time domain reflectometer; HDS, heat dissipator sensor; WM, watermark sensor; MPS-2, dielectric water potential sensor

with small dimensions of the initial landslide. Thickness of ash-fall pyroclastic soil cover was found varying from 3.0 m, close to the landslide main scarp, up to 4.0–5.0 m, in the uppermost investigated area. Within the whole thickness, typical stratigraphic setting was found in a topsoil horizon (A and B horizons) and in alternating pumiceous lapilli horizons (C horizons) and paleosols (Bb horizons). Moreover, a basal paleosol (Bb<sub>basal</sub>) wrapping the carbonate bedrock and filling its open discontinuities was constantly observed. About the land use, a chestnut deciduous wood (*Castanea sativa*) covers the landslide initiation area as it is typical of the most part of peri-Vesuvian mountain slopes. The soil hydrological monitoring station was assembled with 23 tensiometers, four of these provided with PH transducer and automatic datalogger (Spectrum Technologies, Inc.), eight Watermark sensors (Spectrum Technologies, Inc.) and five MPS-2 sensors (Meter) provided with a datalogger (Spectrum Technologies, Inc. and Meter, respectively). All sensors were buried at different depths and located approximately at the middle of each pyroclastic soil horizons, except for the pumiceous lapilli ones whose coarse grain size prevents a reliable hydraulic coupling with the devices (Table 2). To consider the levelled and damped hydrological variability of the deeper soil horizons, sensors were nested into six verticals with a number decreasing with the depth (Fig. 7b). The readings of non-automated tensiometers were carried out by an operator with a weekly frequency, while with 10–15 min periodicity for the other automated instruments. The monitoring activity covered approximately 10 hydrological years, starting from January 2011 to June 2020, with a different data recording periodicity (Fig. 8b). To analyze the effect of rainfall and evapotranspiration processes on the hydrological regime of ash-fall pyroclastic coverings, daily rain and air temperature data were gathered from the Torriello station, located at about 0.8 km from the monitoring station site at about 840 m a.s.l.

Finally, to understand seasonal hydrological behavior of soil covers, Duration Curves (DC) of time series of PH were reconstructed for the M<sub>5</sub> and SM<sub>5</sub> test sites (Fig. 9) (Dalrymple 1960; Stedinger and Cohn 1986; Webb and Betacourt 1992; Helsel and Hirsch 2002). This analysis was supposed fundamental for a comprehensive assessment of the temporal probability (hazard) to landslide triggering by considering the compound probability of assumed antecedent hydrological conditions of soil covers and of a triggering rainfall event with certain intensity and duration values.

### 3.2 Estimation of rainfall thresholds

To assess hydrological conditions controlling the triggering of initial landslides in both study areas, thresholds values based on cumulative amount versus duration of rainfall events ( $E-D$ ) were estimated by deterministic approaches based on a coupled hydrological and slope stability modeling (Fig. 10).

#### 3.2.1 Montuè test site (M<sub>5</sub>)

For the M<sub>5</sub> test site, the hydrological and slope stability modeling was performed considering a detailed reconstruction of the engineering geological model of the slope, including the representative geotechnical and hydrological soil features previously described (Table 1). The modeling was carried out by the TRIGRS model (Baum et al. 2008) which was implemented for the entire slope of the M<sub>5</sub> test site by a 5 m-resolution Digital Elevation Model (DEM) and considering different constant rainfall events with duration varying in the range of 1–200 h and cumulative value varying in the range 1–1000 mm. These



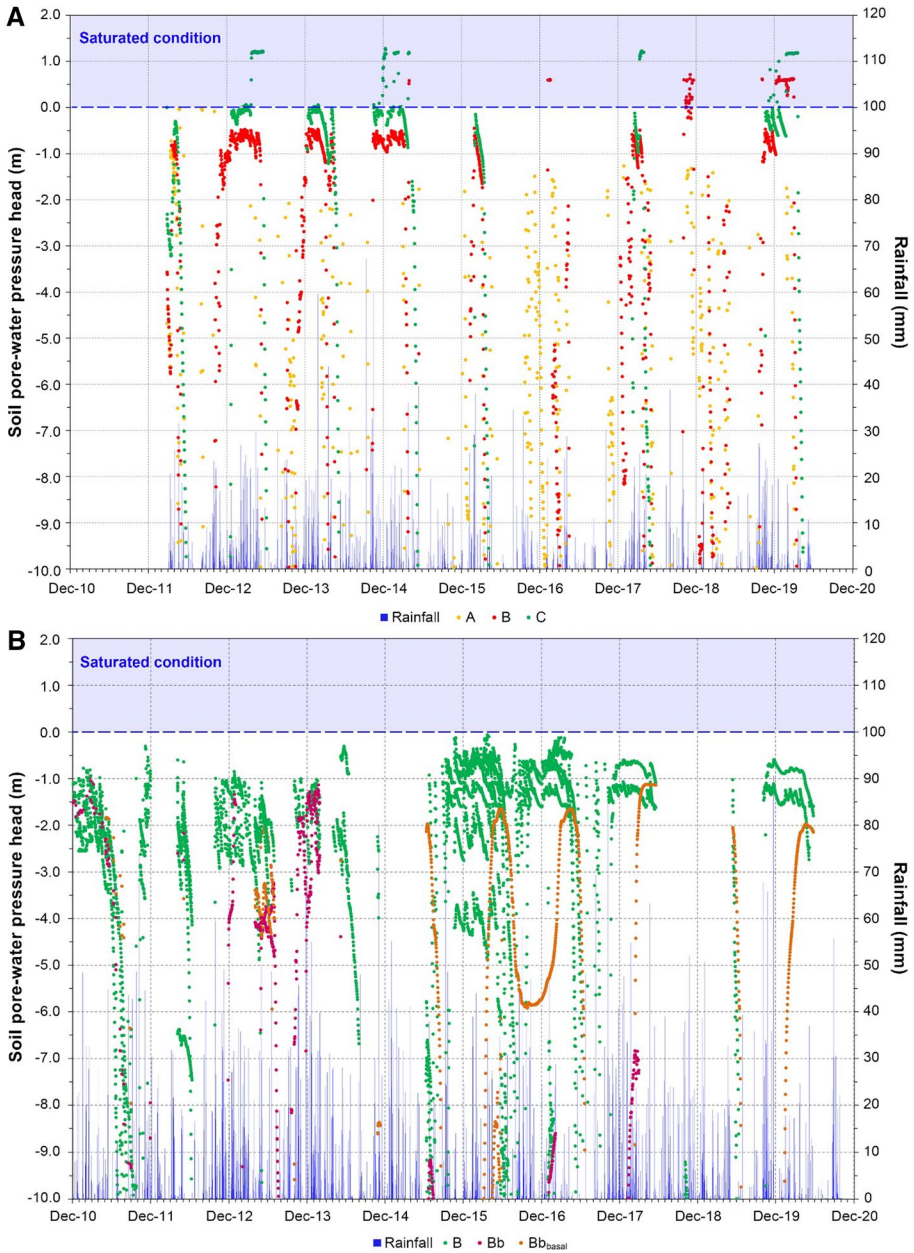


**Fig. 8** (a) Value of PH time series (down to  $-10.0$  m) recorded in the period March 2012–August 2020 in Montuè (Ms) test site; (b) value of PH time series (down to  $-10.0$  m) recorded in the period December 2010–June 2020 in Sarno Mountains (SMs) test site. Data are shown according to soil horizons while the histogram represents daily rainfall data

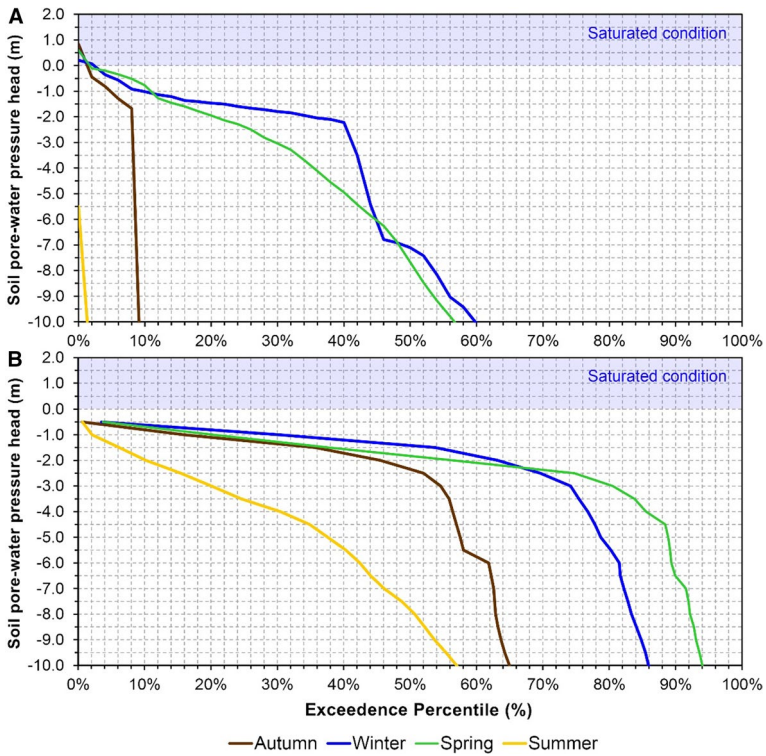
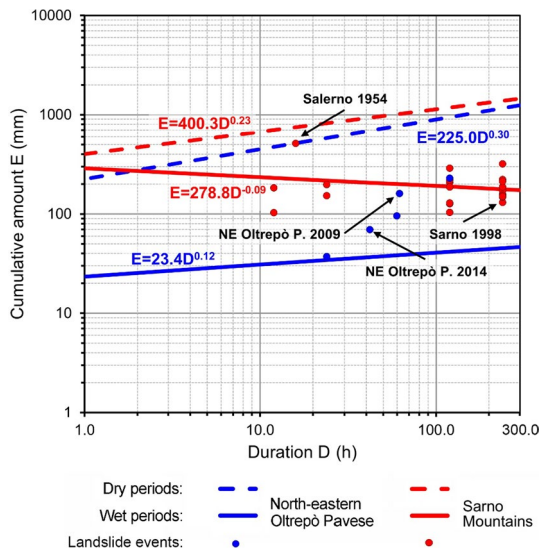


**Fig. 9** Seasonal duration curves (DCs) of mean PH (down to  $-10.0$  m) obtained for Montuè (Ms) (a) and Sarno Mountains (b) (SMs) test sites. Values of PH time series were showed down to  $-10.0$  m

**Fig. 10** Comparison between the cumulative amount—duration rainfall thresholds ( $E-D$ ) derived by hydrological modeling and slope stability analysis of Montuè (Ms) (blue lines) and Sarno Mountains (SMs) (red lines), respectively, for dry (dashed lines) and wet (continuous lines) seasonal antecedent conditions. The rainfall amounts that caused the main landslide events in north-eastern Olterpò Pavese on 2009 and 2014, and the high magnitude debris flow events of Salerno-Amalfi coast (October 1954) and Sarno (May 1998) are also shown



rainfall conditions were considered well matching the typical ones characterizing landslide events of the area during autumn. During the monitored time span, several rainfall events were observed between September and October and characterized with high intensity and short duration (e.g., 13th October 2014, 67 mm fallen in 10 h with a rainfall intensity ranging between 5 and 20 mm/h). Conversely, rainfall events recorded during the late autumn, winter and spring were typically characterized by longer durations (mostly between 30 and 120 h) and a quite constant intensity (mostly 1–4 mm/h).

Each of these rainfall events were simulated considering two antecedent soil hydrological conditions, typical of dry and wet periods, identified through a statistical analysis of the most typical PH values (Bordoni et al. 2019). Results of the hydrological modeling were used to perform slope stability analyses at typical failures depth (1.0 m) within the modeled cover (Bordoni et al. 2015) and accounting for simulated unsaturated soil conditions (Lu and Likos 2006; Lu et al. 2010). These calculations allowed the recognition of critical rainfall duration-cumulative amount conditions leading to shallow landslide triggering (Factor of Safety— $FoS \leq 1$ ), thus discriminating rainfall events with no slope failures ( $FoS > 1$ ). As a result, starting from a dataset of 850 pairs of cumulative rainfall ( $E$ ) and duration ( $D$ ), two rainfall thresholds for dry and wet initial soil conditions were reconstructed, defined by a frequentist method based on a 5% exceedance probability threshold, according to Brunetti et al. (2010). The thresholds were validated considering both rainfall events which triggered or not shallow landslides in the period between August 1992 and August 1997 (Bordoni et al. 2019). However, further validations were carried out considering the location of duration-cumulated amount pairs of four events triggering shallow landslides in  $M_5$  area (April 2009, February–March 2014, December 2019, December 2020).

### 3.2.2 Sarno Mountains test site (SMs)

Hydrological modeling and slope stability analyses carried out for the SMs test area were performed considering detailed engineering geological models reconstructed for source areas of three initial debris slides, whose downslope evolution triggered respective debris flows on the 5th–6th May, 1998 (De Vita et al. 2013). In particular, the slope engineering geological models are related to three representative geomorphological conditions of the initial landslides source areas, corresponding to knickpoints, upper edge of rocky scarps and road cuts. Hydraulic (unsaturated/saturated) and geotechnical parameters previously described (Table 1) were considered to perform hydrological numerical modeling by the VS2DTI finite-difference code (Hsieh et al. 2000). Numerical models were calibrated by monitoring PH time series which were also used to assess representative summer and winter soil hydrological conditions (Fusco and De Vita 2015; Napolitano et al. 2016). Rainfall input, corresponding to in-flux boundary condition, was set with constant values of 2.5, 5.0, 10.0, 20.0 and 40.0 mm/h. Boundary conditions both at the upstream and downstream ends were set as seepage faces, while the contact with the underlying carbonate bedrock as a gravity drainage boundary. Results of numerical modeling, expressed in terms of PH and water content, were used for carrying out slope stability analyses by the simplified Bishop method (Bishop 1955) for each time step of the numerical hydrologic simulation. Moreover, in order to account the effect of unsaturated conditions, slope stability analyses were performed considering the soil effective stress concept developed by Lu and Likos (2006) and Lu et al. (2010). By these calculations, thresholds were derived through interpolation of critical rainfall intensity and duration values leading to slope instability ( $FoS \leq 1$ ). The

validation of the estimated thresholds was carried out by comparison with known rainfall conditions of past landslide events (Tufano et al. 2019).

## 4 Results

### 4.1 Slope hydrological behaviors

During dry summer periods, PH recorded reached very low values in both test sites, exceeding down  $-10.0$  m. Therefore, only parts of both time series with higher values were analyzed in this study (Figs. 8, 9) due to their potentially critical effect on slope stability. The subsequent analysis of PH time series for both the test sites was carried out by the reconstruction of seasonal Duration Curves (DCs), allowing estimation of exceedance frequencies for given values of PH (Fig. 9).

#### 4.1.1 Montuè test site (Ms)

In a preliminary analysis, PH time series for the  $M_S$  test site covered almost seven years, from March 2012 to December 2019 (Fig. 8a). During the rainy periods, occurring typically from November to March, soil hydrological conditions were observed varying from the near saturation ( $PH < -1.0$  m) to saturation ( $PH \geq 0$ ) conditions. Specifically, the latter occurred in the coldest months of the year, from December to May. The higher was the rainfall amount during these months, the longer was the period with conditions close to saturation in the soil covering: 20–35 days with a cumulative rainfall of 241 mm and 138 days with a value of 337 mm. In these conditions, the A and B soil horizons (0.7 m deep) did not get completely saturated, since the highest values of PH monitored at the depth of 0.6 m was of  $-0.3$  m. Instead, the C soil horizon reached saturated conditions with the formation of a water table, as testified by positive PH values ( $0.1 \leq PH \leq 0.5$  m) at the depth of 1.2 m. During the winter months monitored, the occurrence of snow events was not so usual and prolonged in time. Thus, only the infiltration of melted snow may represent a predisposing factor, maintaining soils in a very wet condition until early spring.

Contrarily, in summer months the decrease in the PH was observed faster in the shallower soil horizons than in the deeper ones. In July and August, the driest conditions were observed since PH reached values approximately of  $-10.2$  m in the entire soil profile (not showed in Fig. 8a). Finally, autumn months were considered as a transitional period due to the significant increase in PH because of rainfall events and the decrease in evapotranspiration processes. The re-wetting of the soil profile up the depth of 0.6–0.7 m, with PH values close to  $-1.0$  m, occurred during rainfall events of October and November, while saturation of C soil horizon occurred typically since the end of November when infiltration became more consistent.

The soil cover characterizing the  $M_S$  test site was recognized with the wettest condition during autumn, winter and spring months as it is indicated by the exceedance percentiles of about 1.5% for the saturated condition ( $PH \geq 0$  m) (Fig. 9a). Furthermore, the seasonal behavior of the whole soil cover, winter and spring seasons are characterized by the wettest condition as it can be recognized, respectively, by the exceedance percentiles of 60% and 58% for  $PH > -10$  m. A significant difference between the winter and spring DCs, with a marked knee (exceedance percentile of 40% for  $PH = -2.0$  m) for the first and a regular distribution for the second (exceedance percentile of 20% for  $PH = -2.0$  m), can be

observed. These differences indicate, respectively, an irregular distribution of soil moisture along the soil profile during winter, in favor of shallower soil horizons, and a more regular distribution during spring due to the redistribution of soil moisture at higher depths. In the summer season, exceedance percentile of less than 2% for  $PH > -10$  m and the highest PH value of  $-6.5$  m indicate that the entire soil cover is characterized by a strong drying process. Finally, the angular shape of the DC in the autumn season, with a marked knee at about  $PH = -1.8$  m, corresponding to an exceedance percentile of 8% and  $PH > -10$  m with an exceedance percentile of 9%, show clearly the beginning of the wetting process involving primarily surficial soil horizons.

#### 4.1.2 Sarno Mountains test site (SMs)

For the  $SM_5$  test site, the whole PH time series, recorded over 10 monitoring years, showed a significant seasonal hydrological control (Fig. 8b) characterized by values always ranging in unsaturated conditions and, with different patterns, controlled by the precipitation regime and water losses due to evapotranspiration process. The monitoring allowed the recognition of the PH variability in the range between  $-0.2$  and  $-374.1$  m, thus indicating that saturated conditions were never observed, although conditions of near saturation, not exceeding upward the limit of  $-0.3$  m, were only occasionally recorded. Rainy periods were recognized as characterized by higher PH values, due to the combined effects of higher rainfall and lower evapotranspiration rates. The temporal correspondence between peaks of PH and rainfall events was observed being more direct for shallower soil horizons and damped and delayed for the deeper ones. The shallower soil horizons showed a series of PH peaks correlated directly with rainfall events or following them shortly. Moreover, only the Bb and  $Bb_{\text{basal}}$  soil horizons showed very low PH values with very smoothed and damped peaks. During periods with snow cover, occasionally occurring in February, PH values showed that infiltration process were strongly limited to just the shallowest soil horizons. In the dry period, starting from April until October, PH values, after an initial exponential decrease occurring firstly in the upper part of the ash-fall pyroclastic soil cover and progressively in the deeper zone, ranged between  $-3.2$  and  $-374.1$  m. This behavior was related to the increase in evapotranspiration rate and to the decrease in rainfall events from the late spring to the early autumn. Leaf growth of deciduous chestnut forest occurring during this period was also recognized playing a predominant role on the evapotranspiration demand. Starting from September, corresponding approximately to the end of the dry period, the stop of leaf activity and the occurrence of rainfall events was observed leading to an abrupt increase in PH in the upper part of the ash-fall pyroclastic soil mantle. In this period, although the infiltration front was observed having a progressive deepening through shallower soil horizons, a further decrease in PH in deeper soil horizons was detected.

The whole pyroclastic soil mantle revealed the existence of a constant unsaturated condition through seasons, reaching a near-saturation condition ( $PH = -0.3$  m) as the maximum PH value. An inhomogeneous distribution of PH values during seasons, even if more regular than that of the Ms test site, was recognized. It can be subdivided approximately in three main frequency classes according to PH range considered (Fig. 9b). The first is represented by values comprised from  $-0.5$  m to about  $-2.0$  m for wetter seasons (autumn, winter and spring) and  $-0.5$  m to about  $-4.5$  m for the driest one (summer). The transition to the second frequency class occurs through a marked knee in the DCs with PH values comprised from  $-2.0$  m to about  $-4.0$  m for wetter seasons and  $-4.5$  m to about  $-6.0$  m for the driest one. Finally, the third class has PH values comprised between the preceding

values and the lower limit considered ( $PH = -10.0$  m). In detail, the first class coincides with flat-shaped curves showing similarly a regular and homogeneous hydrological state, more for winter and spring than for autumn seasons. During winter and spring, the ash-fall pyroclastic soil mantle reached exceedance percentiles of 52% and 40% for  $PH \geq -1.5$  m and of 70% and 72% for  $PH \geq -2.5$  m, respectively. Instead, during autumn less similar hydrological condition were observed with exceedance percentiles reaching about 34% for  $PH \geq 1.5$  m and about 52% for  $PH \geq 2.5$  m. Contrastingly, summer season resulted with a steeper DC indicating an inhomogeneous drying process of the whole ash-fall pyroclastic soil cover as it clearly appears from the exceedance percentiles of 8% for  $PH \geq -1.5$  m, 14% for  $PH \geq -2.5$  m and 58% for  $PH \geq -10.0$  m. Wetter conditions, which characterize the ash-fall pyroclastic soil mantle during autumn, winter and spring seasons, is clearly showed by marked knees on the DCs at the transition to the second frequency class. On the contrary, a smoothed knee was observed for the summer season passing from the first to second frequency class. The third class is characterized by DC curves for wetter seasons with a steepness more marked than that of summer.

## 4.2 Rainfall thresholds

Physics-based  $E$ – $D$  rainfall thresholds were reconstructed for both test sites by simulating the effects of rainfall events with different constant intensities and durations till the slope failure and considering representative antecedent soil hydrological conditions, as recognized by PH monitoring time series (Fig. 10).

### 4.2.1 Montuè test site (Ms)

According to typical seasonal PH values (Fig. 9a), physics-based  $E$ – $D$  rainfall thresholds of the Oltrepò Pavese test site were reconstructed considering two initial hydrological statuses of the soil cover. The first one, with  $PH = -1.0$  m, represents a typical transitory condition existing during the wetting process of winter, spring and autumn seasons. The second one, based on the saturated condition ( $PH = 0.0$  m), occurs with a significant frequency in winter, spring and autumn seasons (Fig. 9a). Both  $E$ – $D$  rainfall thresholds reconstructed for the Ms test site are characterized by different steepness and by a marked vertical shift which results in very different values of cumulative rainfall ( $E$ ) for different durations ( $D$ ). Specifically, the  $E$  shift (vertical) indicates that the rainfall threshold, accounting for an initial unsaturated condition ( $PH = -1.0$  m), is highly above than that of the wet period, which relies on initial saturated conditions ( $PH = 0$  m). Consequently, in the first case more severe rainfall  $E$ – $D$  conditions are needed for the triggering of shallow landslides, in comparison with that of the initial saturation case. Comparing the two thresholds, differences in cumulative rainfall ( $E$ ) of about 275, 420 and 750 mm can be assessed for durations ( $D$ ) of 1.0, 10.0 and 100.0 h, respectively.

A validation of deterministic rainfall thresholds estimated for Ms test site was carried out considering rainfall events of the period August 1992–August 1997 (Bordoni et al. 2019) and by calculating indexes of a confusion matrix (true positives, true negatives, false positives, false negatives). For the summer threshold, true negative was of 100% and false positive was of 0%, while for the winter one true positive was of 100% and true negative of 93%, with a respective false positive of 7%. A further validation was carried out considering the main recent events recorded in  $M_s$  area, occurred with saturated conditions of the

soil cover (Zizioli et al. 2013; Bordoni et al. 2015). All these events were located correctly above the  $E$ – $D$  threshold of the wet period (Fig. 10).

#### 4.2.2 Sarno Mountains test site (SMs)

$E$ – $D$  rainfall thresholds obtained for the Sarno Mountains area were reconstructed considering the seasonal effect, thus considering typical winter (wet) and summer (dry) antecedent soil hydrological conditions. The latter correspond to PH representative values (Napoli-tano et al. 2016) ranging, respectively, from  $-1.0$  to  $-0.4$  m and from  $-7.6$  to  $-4.7$  m. Also in this case, a great difference between winter and summer  $E$ – $D$  rainfall thresholds was observed (Fig. 10) resulting in different slope sign and steepness as well as in cumulative amount ( $E$ ) shift. In comparison with the winter  $E$ – $D$  rainfall threshold, the summer one results in a strong increase in the cumulative amount ( $E$ ), which rises with the duration ( $D$ ). Specifically, the differences in cumulative amount ( $E$ ) can be estimated in about 100, 470 and 900 mm for durations ( $D$ ) of 1.0, 10.0 and 100.0 h, respectively. Such a behavior shows clearly a strong shift of  $E$ – $D$  thresholds of the dry season toward higher values of rainfall duration and/or cumulative amount.

The validation of rainfall thresholds estimated for SMs test site was hampered by the availability of known debris flows events, preceding the catastrophic one of May 1998, for which rainfall was mostly measured at rainfall gauges located at lower altitudes, with a high altimetric distance from source areas due to the mountainous features (up to 600 m). For this reason, only a limited selection of landslide occurrences was considered, corresponding to all cases with associated rainfall records characterized by a greater proximity of the rain gauge station. Moreover, the selection was based also on a return period of rainfall greater than 1 years (Tufano et al. 2019), in order to exclude not significant rainfall recordings. Based on such settings, the summer threshold results correctly located above all landslide events considered, even for the cases with a return period greater than 10 years, thus highlighting the extremely relevant role of antecedent soil hydrological conditions in rainfall triggering conditions (Fig. 10). Instead, the winter threshold fairly matches landslide events associated to rainfall with a return period greater than 2 years, indicating some events located above the threshold itself and others below it, the latter being affected by uncertainties in rainfall recordings. These outcomes are also clear by comparing  $E$ – $D$  rainfall conditions which caused the high-magnitude debris flow events of Salerno-Amalfi coast (25th and 26th October 1954) and Sarno Mountains (5th and 6th May 1998), which are, respectively, located in a much higher position and slightly below the winter threshold (Fig. 10).

## 5 Discussion

The comparison of results of soil hydrological monitoring of slopes prone to rainfall-induced shallow landslides in two different geomorphological environments shows the strong control played by geological and geomorphological factors and their effects on rainfall conditions triggering shallow landslides. By a methodological point of view, the soil hydrological monitoring is proved to be a fundamental activity to understand slope hydrological behavior and to model properly slope stability under given antecedent soil hydrological conditions and rainfall events (Mirus et al. 2018b).

A first comparison starts from the climate features of the two test sites, which are characterized by a temperate-mesothermal climate in the case of the  $M_5$  test area, while by a cold-summer Mediterranean climate for the  $SM_5$  one. Such climate differences, joined with the evapotranspiration demand, were found controlling the slope hydrological response of soil covering of the two test sites.

Outcomes of long-lasting soil hydrological monitoring in the  $M_5$  and  $SM_5$  test sites emphasize effects of local geological and hydrological features on the slope hydrological response, thus on the related physics-based rainfall thresholds. Firstly, stratigraphic settings of soil coverings as well as soil hydrological and geotechnical properties were recognized as being strongly controlled by different geological features of the bedrock.

The regolith of the  $M_5$  test site is formed by fine cohesive, from medium-plastic to high-plastic soils, such as clayey sandy silt with sparse pebbles. Instead, ash-fall pyroclastic soils covering the  $SM_5$  test site are heterogeneous in grainsize because varying from loamy sand, in the case of present soil (B soil horizon) and paleosols (Bb soil horizons), to gravel (pumiceous lapilli), which correspond to unweathered C soil horizons.

Very relevant differences were found characterizing hydraulic soil properties.  $M_5$  soil covering is characterized by the lowest values of hydraulic conductivity and a gradual decrease with the depth. Instead, the ash-fall pyroclastic soil mantle of the  $SM_5$  test site is characterized by high contrasts in hydraulic conductivity among the finer pedogenized soil horizons (Bb and  $Bb_{\text{basal}}$ ) and the coarser lapilli pumiceous soil horizons (C soil horizons). Furthermore, by the comparison among Soil Water Retention Curves (SWRCs), soils of the  $SM_5$  test site resulted with a water retention capacity more significant than those of the  $M_5$  test site due to both the prevailing silty fraction and the higher soil water retention properties of pyroclastic soils.

Fundamental understandings of the slope hydrological response derive by the comparison of the PH time series. That measured at the  $M_5$  test site (Bordoni et al. 2015; 2017) shows the frequent occurrence of saturated conditions in winter and spring seasons. In these periods, the combined effect of recurrent rainfall events, lower evapotranspiration rates and lower hydraulic conductivity of soil profile, especially of lower soil horizons, favor the increase in water content up to saturation (Alessio 2019; Watakabe and Matsushi 2019).

Differently the  $SM_5$  test site shows (Fusco and De Vita 2015) dominant unsaturated conditions, thus according to preceding measurements (Greco et al. 2013). In this test site, a delayed and dumped dynamics of PH values is observed between the shallower soil horizons (B and Bb soil horizons) and the deeper one ( $Bb_{\text{basal}}$  soil horizon). Specifically, the deeper soil horizons were observed with the lowest PH values approximately at the beginning of the spring (March–April), thus showing a temporally shifted hydrological regime in comparison with that of the shallower soil horizons. As a matter of fact, the lowering of PH value for the shallower soil horizons occurs since the beginning of the rainy season (October–November). A gradual deepening of the infiltration front was observed to be strongly controlled by capillary barrier effects existing at the top of coarser pumiceous lapilli horizons (Mancarella et al. 2012; Fusco et al. 2017) and the general progressive decrease in saturated hydraulic conductivity with depth (De Vita et al. 2013).

Since the late spring until the early autumn, the decreasing of rainfall events and the increasing of evapotranspiration rate cause a strong decrease in PH values. Lowering of PH values occurs more gradually in the  $M_5$  test site than in the  $SM_5$  one, where the soil moisture is strongly reduced by the higher evapotranspiration demand due to the deciduous forest (*Castanea Sativa*). Very dry conditions characterize the soil coverings



during summer periods, whose occasional lowering of PH values in the shallowest part is strongly related to the occurrence of sporadic rainfall events.

By the analysis of DCs it is possible to assess that the major probability for a landslide triggering for the  $M_S$  test site occurs mainly from autumn to spring, with an annual exceedance percentile of about 5%. In these cases, heavy rainfall events cause a further increase in PH, up to positive values of 0.2–0.5 m, as it is testified by the water table rise in deeper soil horizons during months of the wet periods. Specifically, saturated conditions and positive PH can develop in B soil horizon, reaching a depth from the ground up to 0.7–0.8 m, therefore causing conditions critical for landslide triggering. Such similar hydrological conditions are recognized in many similar frameworks of the world (Smethurst et al. 2012; Fressard et al. 2016; Mirus et al. 2018b). Contrastingly, saturation was never observed for the  $SM_S$  test site and critical conditions for slope stability were recognized occurring principally during winter and spring, when PH ranges above the value of  $-2.0$  m, but below  $-0.3$  m, with an exceedance percentile greater than 50%. In these cases, heavy rainfall events, causing infiltration within the ash-fall pyroclastic soil covering, lead to the increase in unsaturated hydraulic conductivity in the upper soil horizon thus promoting unsaturated throughflow and the downslope formation of saturation wedges at hydrogeological discontinuities corresponding to a decrease in hydraulic transmissivity (Reid et al. 1988; De Vita et al. 2013; Tufano et al. 2021).

During the dry period, from the late spring to the late summer, more stable conditions can be assumed for both test sites due to lower antecedent PH values and low probability of heavy and/or prolonged rainfall events. Furthermore, transitory conditions were recognized occurring in autumn and winter, with high PH values in the shallower soil horizons and still lower values in the deeper ones. In these transitory periods the probability of landslide triggering can be considered intermediate.

The soil hydrological monitoring allowed to recognize complex hydrological regimes characterizing the soil mantles of both test sites and their dependence on local geological, geomorphological and climatic features. Therefore, such finding opens new perspectives in the understanding of limits and uncertainties of empirical rainfall thresholds (Nikolopoulos et al. 2014), which are reconstructed on the basis of inhomogeneous and incomplete landslide inventories, uncertain rainfall recordings and, in most of the cases, not considering antecedent hydrological conditions. Therefore, the estimation of rainfall thresholds based on physics-based approaches is fundamental to reduce such uncertainties (Mirus et al. 2018b), especially for landslide rainfall thresholds reconstructed for specific and homogeneous geomorphological frameworks. Accordingly, the comparison among physics-based rainfall thresholds of both test sites is an important achievement for understanding the control of local geological, geomorphologic, geotechnical and hydrological features on rainfall conditions needed for the landslide triggering.

Rainfall thresholds of both wet and dry periods (Fig. 10) show a relevant shift in rainfall cumulative amount ( $E$ ), which accounts for the control of local geotechnical and hydrological conditions, both depending on local geological and geomorphological features. Considering the rainfall thresholds of the wet period, that of the  $SM_S$  test site is markedly higher than that of the  $M_S$  test site, with differences of about 275, 220 and 160 mm for the durations ( $D$ ) of 1.0, 10.0 and 100.0 h. Interestingly, the slope of the  $SM_S$  rainfall threshold is slightly negative indicating a strong decrease in rainfall intensity for longer durations. This unusual trend can be related to antecedent wet soil conditions reached during prolonged and low-intensity rainfall events, which require a total rainfall amount, to reach slope instability, lower than that needed for drier antecedent conditions.

Similarly, the comparison between rainfall thresholds of the dry period shows greater  $E$  values for the SMs rainfall threshold with differences of about 195, 200 and 250 mm for the durations ( $D$ ) of 1.0, 10.0 and 100.0 h.

Approach and results proposed can be conceived as reliable for setting EWS system at least for the site-specific scale for both study areas. Since a slight change in soil features or slope settings (e.g., soil thickness or soil physical and hydrological features; slope angle) could result in variability of rainfall thresholds, the results obtained can be extended at distributed scale only if the analyzed test-sites are representative of geological, pedological, hydrological and geomorphological features of that sector. Accordingly, another way to extend the results to an area larger than the site-specific scale is to consider, in the computation of the physics-based models, the possible heterogeneities of slope physical features and their effects in the estimation of rainfall thresholds, through a sensitivity and probabilistic analysis (e.g., Marin and Velásquez 2020).

## 6 Conclusions

Assessing hazards related to rainfall-induced shallow landslides is a challenging task for the risk management of urbanized areas which are potentially exposed to landslide effects, thus deserving careful estimations aimed at setting up of reliable EWSs. With such a purpose, efforts must be made for reducing uncertainties related to the assessment of critical hydrological conditions leading to the initiation of shallow landslides and to minimize their dangerous misestimations.

In this paper, a comparison between results of soil hydrological monitoring and estimation of physics-based  $E$ - $D$  rainfall thresholds of two distinct geomorphological environments with a high proneness to shallow landsliding and contrasting geological and geotechnical characteristics was carried out. Therefore, the comparison between these two test sites was motivated not by similarity but difference in geological and geotechnical characteristics in order to assess their effect on slope hydrological response and conditions leading to landsliding.

The principal outcome of this comparison is the clear understanding of the role played by local geotechnical and hydrological characteristics, controlled by local geological, geomorphological and climatic features, on threshold rainfall values. Therefore, the proposed physics-based approach, based on geological and geotechnical characterization, field soil hydrological monitoring and coupled hydrological and slope stability modeling, is demonstrated to be feasible and reliable in reducing uncertainties related to the empirical approach.

In conclusion, the physics-based approach proposed for estimating the  $E$ - $D$  rainfall thresholds, if based on accurate geological and geotechnical characterizations as well as on field soil hydrological monitoring, can be considered as an alternative to the empirical one and useful for assessing different landslide hazard levels related to seasonality.

Furthermore, the results obtained at the site-specific scale and the derived rainfall thresholds can be implemented in an EWS potentially extendable at the distributed scale (catchment or larger) by considering in computations the spatial variability of model parameters in a general framework of homogeneous geological, geomorphological and geotechnical conditions. Finally, the deterministic approach is proposed as a possible way to estimate landslide hazards and set EWS in all cases in which empirical models are of difficult applicability due the incompleteness of landslide inventory, inconsistency of

landslide records, unreliability of rainfall recordings and indetermination of antecedent soil hydrological conditions.

**Funding** Open access funding provided by Università degli Studi di Pavia within the CRUI-CARE Agreement. This research was funded by the Governmental Commissariat for the hydrological emergency in the Campania region (Act No. 1902 of 25 September 2001) and the Ph.D. Program (2014 – 2018) of the Department of Earth, Environmental and Resources Sciences (DiSTAR), University of Naples Federico II. Moreover, it has received funding in the framework of the ANDROMEDA project, which has been supported by Cariplo Foundation, Grant No. 2017-0677.

## Declarations

**Conflict of interest** The authors have no conflicts of interest to declare that are relevant to the content of this paper.

**Open Access** This article is licensed under a Creative Commons Attribution 4.0 International License, which permits use, sharing, adaptation, distribution and reproduction in any medium or format, as long as you give appropriate credit to the original author(s) and the source, provide a link to the Creative Commons licence, and indicate if changes were made. The images or other third party material in this article are included in the article's Creative Commons licence, unless indicated otherwise in a credit line to the material. If material is not included in the article's Creative Commons licence and your intended use is not permitted by statutory regulation or exceeds the permitted use, you will need to obtain permission directly from the copyright holder. To view a copy of this licence, visit <http://creativecommons.org/licenses/by/4.0/>.

## References

- Alessio P (2019) Spatial variability of saturated hydraulic conductivity and measurement-based intensity-duration thresholds for slope stability, Santa Ynez Valley, CA. *Geomorphology* 342:103–116. <https://doi.org/10.1016/j.geomorph.2019.06.004>
- Baum RL, Savage WZ, Godt JW (2008) TRIGRS—a Fortran program for transient rainfall infiltration and grid-based regional slope-stability analysis, version 2.0. Open-file report 2008-1159, Savage WZ, Ed, US Geological Survey, Denver, CO, USA
- Bishop AW (1955) The use of the slip circle in the stability analysis of slopes. *Geotechnique* 5(1):7–17. <https://doi.org/10.1680/geot.1955.5.1.7>
- Bogaard T, Greco R (2016) Landslide hydrology: from hydrology to pore pressure. *Wires Water* 3:439–459. <https://doi.org/10.1002/wat2.1126>
- Bogaard T, Greco R (2018) Invited perspectives: hydrological perspectives on precipitation intensity-duration thresholds for landslide initiation: proposing hydro-meteorological thresholds. *Nat Hazard* 18(1):31–39. <https://doi.org/10.5194/nhess-18-31-2018>
- Bordoni M, Meisina C, Valentino R, Lu N, Bittelli M, Chersich S (2015) Hydrological factors affecting rainfall-induced shallow landslides: from the field monitoring to a simplified slope stability analysis. *Eng Geol* 193:19–37. <https://doi.org/10.1016/j.enggeo.2015.04.006>
- Bordoni M, Bittelli M, Valentino R, Chersich S, Meisina C (2017) Improving the estimation of complete field soil water characteristic curves through field monitoring data. *J Hydrol* 552:283–305. <https://doi.org/10.1016/j.jhydrol.2017.07.004>
- Bordoni M, Corradini B, Lucchelli L, Valentino R, Bittelli M, Vivaldi V, Meisina C (2019) Empirical and physically based thresholds for the occurrence of shallow landslides in a prone area of northern Italian Apennines. *Water* 11(12):2653. <https://doi.org/10.3390/w11122653>
- Bordoni M, Inzaghi F, Vivaldi V, Valentino R, Bittelli M, Meisina C (2021) A data-driven method for the temporal estimation of soil water potential and its application for shallow landslides prediction. *Water* 13:1208. <https://doi.org/10.3390/w13091208>
- Brunetti MT, Peruccacci S, Rossi M, Luciani S, Valigi D, Guzzetti F (2010) Rainfall thresholds for the possible occurrence of landslides in Italy. *Nat Hazards Earth Syst Sci* 10(3):447–458
- Caine N (1980) The rainfall intensity-duration control of shallow landslides and debris flows. *Geogr Ann Ser A Phys Geogr* 62(1/2):23–27. <https://doi.org/10.2307/520449>

- Calcaterra D, Parise M, Palma B, Pelella L (1999) The May 5th, 1998, landsliding event in Campania (Southern Italy): inventory of slope movements in the Quindici area. In: Proceedings of the international symposium on slope stability engineering, Shikoku, Japan, November 8–11, 1999, vol 2, pp 1361–1366
- Campbell RH (1975) Soil slips, debris flows, and rainstorms in the Santa Monica Mountains and vicinity, southern California, vol 851. US Government Printing Office, New York. <https://doi.org/10.3133/pp851>
- Cannon SH, Gartner JE (2005) Wildfire-related debris flow from a hazards perspective. In: Debris-flow hazards and related phenomena. Springer Praxis Books. Springer, Berlin, pp 363–385. [https://doi.org/10.1007/3-540-27129-5\\_15](https://doi.org/10.1007/3-540-27129-5_15)
- Collins BD, Znidarcic D (2004) Stability analyses of rainfall induced landslides. *J Geotech Geoenviron Eng* 130(4):362–372. [https://doi.org/10.1061/\(ASCE\)1090-0241\(2004\)130:4\(362\)](https://doi.org/10.1061/(ASCE)1090-0241(2004)130:4(362))
- Comegna L, Damiano E, Greco R, Guida A, Olivares L, Picarelli L (2016) Field hydrological monitoring of a sloping shallow pyroclastic deposit. *Can Geotech J* 53(7):1125–1137. <https://doi.org/10.1139/cgj-2015-0344>
- Crosta GB, Dal Negro P (2003) Observations and modelling of soil slip-debris flow initiation processes in pyroclastic deposits: the Sarno 1998 event. *Nat Hazard* 3(1/2):53–69. <https://doi.org/10.5194/nhess-3-53-2003>
- Crosta GB, Agliardi F, Rivolta C, Alberti S, Dei Cas L (2017) Long-term evolution and early warning strategies for complex rockslides by real-time monitoring. *Landslides* 14:1615–1632. <https://doi.org/10.1007/s10346-017-0817-8>
- Crozier MJ (1986) Landslides—causes, consequences and environment. Croom Helm, London, p 252
- Crozier MJ, Eyles RJ (1980) Assessing the probability of rapid mass movement. In: Third Australia–New Zealand conference on geomechanics, Wellington, New Zealand - Institute of Engineers, proceedings of technical groups, vol 6(1) part 1
- Cruden D M, Varnes DJ (1996) Landslide types and processes. In: Landslides: investigation and mitigation. Chapter 3-landslide types and processes. Transportation Research Board special report, p 247
- Dahal RK, Hasegawa S (2008) Representative rainfall thresholds for landslides in the Nepal Himalaya. *Geomorphology* 100:429–443. <https://doi.org/10.1016/j.geomorph.2008.01.014>
- Dalrymple T (1960) Flood-frequency analyses. Geological Survey, Water, 1960-Supply Paper, 1543-A
- De Luca DL, Versace P (2017) A comprehensive framework for empirical modeling of landslides induced by rainfall: the Generalized FLaR Model (GFM). *Landslides* 14(3):1009–1030. <https://doi.org/10.1007/s10346-016-0768-5>
- De Vita P, Nappi M (2013) Regional distribution of ash-fall pyroclastic deposits in Campania (southern Italy) for landslide susceptibility assessment. In: Margottini C, Canuti P, Sassa K (eds) *Landslide science and practice. Spatial analysis and modelling*, vol 3. Springer, Berlin, pp 103–110
- De Vita P, Piscopo V (2002) Influences of hydrological and hydrogeological conditions on debris flows in peri-vesuvian hillslopes. *Nat Hazards Earth Syst Sci* 2(1/2):27–35. <https://doi.org/10.5194/nhess-2-27-2002>
- De Vita P, Reichenbach P, Bathurst JC, Borga M, Crozier GM, Glade T, Guzzetti F, Hansen A, Wasowski J (1998) Rainfall-triggered landslides: a reference list. *Environ Geol* 35:219–233
- De Vita P, Agrello D, Ambrosino F (2006) Landslide susceptibility assessment in ash-fall pyroclastic deposits surrounding Mount Somma-Vesuvius: application of geophysical surveys for soil thickness mapping. *J Appl Geophys* 59:126–139. <https://doi.org/10.1016/j.jappgeo.2005.09.001>
- De Vita P, Napolitano E, Godt JW, Baum RL (2013) Deterministic estimation of hydrological thresholds for shallow landslide initiation and slope stability models: case study from the Somma-Vesuvius area of southern Italy. *Landslides* 10(6):713–728. <https://doi.org/10.1007/s10346-012-0348-2>
- De Vita P, Fusco F, Tufano R, Cusano D (2018) Seasonal and event-based hydrological and slope stability modeling of pyroclastic fall deposits covering slopes in Campania (Southern Italy). *Water* 10(9):1140. <https://doi.org/10.3390/w100911400>
- Del Soldato M, Pazzi V, Segoni S, De Vita P, Tofani V, Moretti S (2018) Spatial modeling of pyroclastic cover deposit thickness (depth to bedrock) in peri-volcanic areas of Campania (southern Italy). *Earth Surf Proc Land* 43(9):1757–1767
- Di Crescenzo G, Santo A (2005) Debris slides-rapid earth flow in the carbonate massifs of the Campania region (Southern Italy): morphological and morphometric data for evaluating triggering susceptibility. *Geomorphology* 66:255–276. <https://doi.org/10.1016/j.geomorph.2004.09.015>
- Esposito E, Porfido S, Violante C (2004) Il nubifragio dell'ottobre 1954 a Vietri sul Mare-Costa di Amalfi, Salerno (No. 2870). CNR-GNDCI-IAMC.120

- Fiorillo F, Guadagno F, Aquino S, De Blasio A (2001) The December 1999 Cervinara landslides: further debris flows in the pyroclastic deposits of Campania (southern Italy). *Bull Eng Geol Environ* 60(3):171–184. <https://doi.org/10.1007/s100640000093>
- Fressard M, Maquaire O, Thiery Y, Davidson R, Llissak C, (2016) Multi-method characterisation of an active landslide: case study in the Pays d’Auge plateau (Normandy, France). *Geomorphology* 270:22–39. <https://doi.org/10.1016/j.geomorph.2016.07.001>
- Fuhrmann CM, Konrad CE II, Band LE (2008) Climatological perspectives on the rainfall characteristics associated with landslides in western North Carolina. *Phys Geogr* 29(4):289–305. <https://doi.org/10.2747/0272-3646.29.4.289>
- Fusco F, De Vita P (2015) Hydrological behaviour of ash-fall pyroclastic soil mantled slopes of the Sarno Mountains (Campania-southern Italy). *Rendiconti Oline Società Geologica Italiana* 35:148–151. <https://doi.org/10.3301/ROL.2015.86>
- Fusco F, De Vita P, Napolitano E, Allocca V, Manna F (2013) Monitoring the soil suction regime of landslide-prone ash-fall pyroclastic deposits covering slopes in the Sarno area (Campania-southern Italy). *Rendiconti Online Società Geologica Italiana* 24:146–148
- Fusco F, Allocca V, De Vita P (2017) Hydro-geomorphological modelling of ash-fall pyroclastic soils for debris flow initiation and groundwater recharge in Campania (southern Italy). *CATENA* 158:235–249. <https://doi.org/10.1016/j.catena.2017.07.010>
- Fusco F, De Vita P, Mirus BB, Baum RL, Allocca V, Tufano R, Di Clemente E, Calcaterra D (2019) Physically based estimation of rainfall thresholds triggering shallow landslides in volcanic slopes of southern Italy. *Water* 11(9):1915. <https://doi.org/10.3390/w11091915>
- Galanti Y, Barsanti M, Cevasco A, Avanzi GDA, Giannecchini R (2018) Comparison of statistical methods and multi-time validation for the determination of the shallow landslide rainfall thresholds. *Landslides* 15:937–952. <https://doi.org/10.1007/s10346-017-0919-3>
- Gariano SL, Brunetti MT, Iovine G, Melillo M, Peruccacci S, Terranova O, Vennari C, Guzzetti F (2015) Calibration and validation of rainfall thresholds for shallow landslide forecasting in Sicily, southern Italy. *Geomorphology* 228:653–665. <https://doi.org/10.1016/j.geomorph.2014.10.019>
- Gariano SL, Melillo M, Peruccacci S, Brunetti MT (2020) How much does the rainfall temporal resolution affect rainfall thresholds for landslide triggering? *Nat Hazards* 100:655–670. <https://doi.org/10.1007/s11069-019-03830-xvxc>
- Geiger R (1954) *Klassifikation der climate nach W. Köppen. Landolt-Börnstein-Zahlenwerte und Funktionenaus Physik, Chemie, Astronomie, Geophysik und Technik*, vol 3. Springer, Berlin, pp 603–607
- Glade T, Crozier M, Smith P (2000) Applying probability determination to refine landslide-triggering rainfall thresholds using an empirical “antecedent daily rainfall model.” *Pure Appl Geophys* 157:1059–1079. <https://doi.org/10.1007/s000240050017>
- Godt JW, Baum RL, Chleborad AF (2006) Rainfall characteristics for shallow landsliding in Seattle, Washington, USA. *Earth Surf Process Landf* 31(1):97–110. <https://doi.org/10.1002/esp.1237>
- Godt JW, Schulz WH, Baum RL, Savage WZ (2008) Modeling rainfall conditions for shallow landsliding in Seattle, Washington. In: Baum RL, Godt JW, Highland LM (eds) *Landslides and engineering geology of the Seattle, Washington, Area*, vol 20. Geological Society of America Reviews in Engineering Geology, Berlin, pp 137–152
- Greco R, Comegna L, Damiano E, Guida A, Olivares L, Picarelli L (2013) Hydrological modelling of a slope covered with shallow pyroclastic deposits from field monitoring data. *Hydrol Earth Syst Sci* 17(10):4001–4013. <https://doi.org/10.5194/hess-17-4001-2013>
- Guadagno FM, Forte R, Revellino P, Fiorillo F, Focareta M (2005) Some aspects of the initiation of debris avalanches in the Campania Region: the role of morphological slope discontinuities and the development of failure. *Geomorphology* 66(1–4):237–254. <https://doi.org/10.1016/j.geomorph.2004.09.024>
- Guadagno FM, Revellino P, Grelle G (2011) The 1998 Sarno landslides: conflicting interpretations of a natural event. In: *International conference on debris-flow hazards mitigation: mechanics, prediction, and assessment, proceedings*, pp 71–81
- Guo Z, Yin K, Gui L, Liu Q, Huang F, Wang T (2019) Regional rainfall warning system for landslides with creep deformation in Three Gorges using a statistical black box model. *Sci Rep* 9:8962. <https://doi.org/10.1038/s41598-019-45403-9>
- Guzzetti F, Peruccacci S, Rossi M, Stark CP (2007) Rainfall threshold for the initiation of landslide in central and southern Europe. *Meteorol Atmos Phys* 98:239–267. <https://doi.org/10.1007/s00703-007-0262-7>
- Guzzetti F, Peruccacci S, Rossi M, Stark CP (2008) The rainfall intensity-duration control of shallow landslides and debris flows: an update. *Landslides* 5(1):3–17. <https://doi.org/10.1007/s10346-007-0112-1>
- Helsel DR, Hirsch RM (2002) *Statistical methods in water resources*. Tech Water Resour Investig U S Geol Surv 4:510

- Howard TR, Baldwin JE II, Donley HF (1988) Landslides in Pacifica, California, caused by the storm. Landslides, Floods and Marine Effects of the Storm of January 3–5, 1982, in the San Francisco Bay Region. California 1434:163–184
- Hsieh PA, Wingle W, Healy RW (2000) VS2DI—a graphical software package for simulating fluid flow and solute or energy transport in variably saturated porous media. US Geological Survey, Water-Resources, Investigations Report 9-4130
- Hungr O, Evans SG, Bovis MJ, Hutchinson JN (2001) A review of the classification of landslides of flow type. *Environ Eng Geosci* 7:221–238. <https://doi.org/10.2113/gseengeosci.7.3.221>
- Hungr O, Leroueil S, Picarelli L (2014) The Varnes classification of landslide types, an update. *Landslides* 11(2):167–194. <https://doi.org/10.1007/s10346-013-0436-y>
- Innes JL (1983) Debris flows. *Prog Phys Geogr Earth Environ* 7:469–501. <https://doi.org/10.1177/03091338300700401>
- IUSS Working Group WRB. World reference base for soil resources 2014. International soil classification system for naming soils and creating legends for soil maps. World soil resources reports No. 106, FAO, Rome
- Jakob M, Hungr O (2005) Debris-flow hazards and related phenomena, vol 739. Springer, Berlin
- Jibson RW (1989) Debris flow in southern Porto Rico. *Geol Soc Am Spec Pap* 236:29–55
- Kim SK, Hong WP, Kim YM (1991) Prediction of rainfall triggered landslides in Korea. In: Bell DH (ed) *Landslides*, vol 2. AA Balkema, Rotterdam, pp 989–994
- Kim JH, Jeong SS, Kim YM, Lee KW (2013) Proposal of design method for landslides considering antecedent rainfall and in-situ matric suction. *J Korean Geotech Soc* 29(12):11–24
- Kim SW, Chun KW, Kim M, Catani F, Choi B, Seo JI (2021) Effect of antecedent rainfall conditions and their variations on shallow landslide-triggering rainfall thresholds in South Korea. *Landslides* 18(2):569–582. <https://doi.org/10.1007/s10346-020-01505-4>
- Köppen W (1936) Das geographische System der Klimate. In: Köppen W, Geiger R (eds) *Handbuch der Klimatologie*. Gebrüder Borntraeger, Berlin, pp 1–44
- Lu N, Godt JW (2013) *Hillslope hydrology and stability*. Cambridge University Press, New York
- Lu N, Likos WJ (2006) Suction stress characteristic curve for unsaturated soil. *J Geotech Geoenviron* 132(2):131–142. [https://doi.org/10.1061/\(ASCE\)1090-0241\(2006\)132:2\(131\)](https://doi.org/10.1061/(ASCE)1090-0241(2006)132:2(131))
- Lu N, Godt JW, Wu DT (2010) A closed-form equation for effective stress in unsaturated soil. *Water Resour Res*. <https://doi.org/10.1029/2009WR008646>
- Mancarella D, Doglioni A, Simeone V (2012) On capillary barrier effects and debris slide triggering in unsaturated layered covers. *Eng Geol* 147–148:14–27
- Marin RJ, Velásquez MF (2020) Influence of hydraulic properties on physically modelling slope stability and the definition of rainfall thresholds for shallow landslides. *Geomorphology* 351:106976. <https://doi.org/10.1016/j.geomorph.2019.106976>
- Melillo M, Brunetti MT, Peruccacci S, Gariano SL, Guzzetti F (2016) Rainfall thresholds for the possible landslide occurrence in Sicily (Southern Italy) based on the automatic reconstruction of rainfall events. *Landslides* 13(1):165–172. <https://doi.org/10.1007/s10346-015-0630-1>
- Melillo M, Brunetti MT, Peruccacci S, Gariano SL, Roccati A, Guzzetti F (2018) CTRL-T: a tool for the automatic calculation of rainfall thresholds for landslide occurrence. *Environ Model Softw* 105:230–243. <https://doi.org/10.1016/j.envsoft.2018.03.024>
- Mirus BB, Mowphew M, Smith J (2018a) Developing hydro-meteorological thresholds for shallow landslide initiation and early warning. *Water* 10(9):1274. <https://doi.org/10.3390/w10091274>
- Mirus BB, Becker RE, Baum RL, Smith JB (2018b) Integrating real-time subsurface hydrologic monitoring with empirical rainfall thresholds to improve landslide early warning. *Landslides* 15(10):1909–1919. <https://doi.org/10.1007/s10346-018-0995-z>
- Mitchell JK, Soga K (2005) *Fundamentals of soil behavior*, vol 3. Wiley, New York
- Moser M, Hohensinn F (1983) Geotechnical aspects of soil slips in Alpine regions. *Eng Geol* 19(3):185–211. [https://doi.org/10.1016/0013-7952\(83\)90003-0](https://doi.org/10.1016/0013-7952(83)90003-0)
- Napolitano E, Fusco F, Baum RL, Godt JW, De Vita P (2016) Effect of antecedent-hydrological conditions on rainfall triggering of debris flows in ash-fall pyroclastic mantled slopes of Campania (southern Italy). *Landslides* 13(5):967–983. <https://doi.org/10.1007/s10346-015-0647-5>
- Nikolopoulos EI, Crema S, Marchi L, Marra F, Guzzetti F, Borga M (2014) Impact of uncertainty in rainfall estimation on the identification of rainfall thresholds for debris flow occurrence. *Geomorphology* 221:286–297. <https://doi.org/10.1016/j.geomorph.2014.06.015>
- Patacca E, Scandone P (2007) Geological interpretation of the CROP-04 seismic line (Southern Apennines, Italy). *Boll Soc Geol It* 7:297–315
- Peres DJ, Cancelliere A (2014) Derivation and evaluation of landslide-triggering thresholds by a Monte Carlo approach. *Hydrol Earth Syst Sci* 18:4913–4931. <https://doi.org/10.5194/hess-18-4913-2014>

- Peres DJ, Cancelliere A, Greco R, Bogaard TA (2017) Influence of uncertain identification of triggering rainfall on the assessment of landslide early warning thresholds. *Nat Hazard* 18:633–646. <https://doi.org/10.5194/nhess-2017-328>
- Piciullo L, Calvello M, Cepeda JM (2018) Territorial early warning systems for rainfall-induced landslides. *Earth Sci Rev* 179:228–247. <https://doi.org/10.1016/j.earscirev.2018.02.013>
- Rahardjo H, Li XW, Toll DG, Leong EC (2001) The effect of antecedent rainfall on slope stability. In: Unsaturated soil concepts and their application in geotechnical practice. Springer, Netherlands, pp 371–399
- Reid ME, Nielsen HJP, Dreiss SJ (1988) Hydrologic factors triggering a shallow hillslope failure. *Bull Assoc Eng Geol* 25(3):349–362. <https://doi.org/10.2113/gseegeosci.xv.3.349>
- Rosi A, Lagomarsino D, Rossi G, Segoni S, Battistini A, Casagli N (2015) Updating EWS rainfall thresholds for the triggering of landslides. *Nat Hazards* 78(1):297–308. <https://doi.org/10.1007/s11069-015-1717-7>
- Rosi A, Segoni S, Canavesi V, Monni A, Gallucci A, Casagli N (2021) Definition of 3D rainfall thresholds to increase operative landslide early warning system performances. *Landslides* 18:1045–1057. <https://doi.org/10.1007/s10346-020-01523-2>
- Rossi M, Peruccacci S, Brunetti MT, Marchesini I, Luciani S, Ardizzone F, Balducci V, Bianchi C, Cardinali M., Fiorucci F, Mondini AC, Reichenbach P, Salvati P, Santangelo M, Bartolini D, Gariano SL, Palladino M, Vessia G, Viero A, Antronico L, Borselli L, Deganutti AM, Iovine G, Luino F, Parise M, Polemio M, Guzzetti, Tonelli G (2012) SANF: National warning system for rainfall-induced landslides in Italy. In: Eberhardt E, Froese C, Turner AK, Lerouil S (Eds) *Landslides and engineered slopes. Protecting society through improved understanding*. Proceedings 11th international symposium on landslides, Banff (Canada), 3–8 June 2012, vol 2, pp 1895–1899
- Segoni S, Rosi A, Rossi G, Catani F, Casagli N (2014a) Analysing the relationship between rainfalls and landslides to define a mosaic of triggering thresholds for regional-scale warning systems. *Nat Hazard* 14:2637–2648. <https://doi.org/10.5194/nhess-14-2637-2014>
- Segoni S, Rossi G, Rosi A, Catani F (2014b) Landslides triggered by rainfall: a semiautomated procedure to define consistent intensity–duration thresholds. *Comput Geosci* 63:123–131. <https://doi.org/10.1016/j.cageo.2013.10.009>
- Segoni S, Piciullo L, Gariano SL (2018) A review of the recent literature on rainfall thresholds for landslide occurrence. *Landslides* 15:1483–1501. <https://doi.org/10.1007/s10346-018-0966-4>
- Side RC, Ochiai H (2006) *Landslides: processes, prediction, and land use*. American Geophysical Union, Washington, DC
- Smethurst JA, Clarke D, Powrie W (2012) Factors controlling the seasonal variation in soil water content and pore water pressures within a lightly vegetated clay slope. *Géotechnique*. <https://doi.org/10.1680/geot.10.p.097>
- Stedinger JR, Cohn T (1986) Flood frequency analysis with historical and paleoflood information. *Water Res* 22:785–793. <https://doi.org/10.1029/WR022i005p00785>
- Terlien MTJ (1998) The determination of statistical and deterministic hydrological landslide-triggering thresholds. *Environ Geol* 35:124–130. <https://doi.org/10.1007/s002540050299>
- Terribile F, Basile A, De Mascellis R, di Gennaro A, Mele G, Vingiani S (2000) I suoli delle aree di crisi di Quindici e Sarno: proprietà e comportamenti in relazione ai fenomeni franosi del 1998. *Quaderni Di Geologia Applicata* 7(1):59–79 (**In Italian**)
- Thomas MA, Mirus BB, Collins BD (2018) Identifying physics-based thresholds for rainfall-induced landsliding. *Geophys Res Lett* 45(18):9651–9661. <https://doi.org/10.1029/2018GL079662>
- Tien Bui D, Pradhan B, Lofman O, Revhaug I, Dick ØB (2013) Regional prediction of landslide hazard using probability analysis of intense rainfall in the Hoa Binh province, Vietnam. *Nat Hazards* 66:707–730. <https://doi.org/10.1007/s11069-012-0510-0>
- Toscani G, Seno S, Fantoni R, Rogledi S (2006) Geometry and timing of deformation inside a structural arc; the case of the western Emilian folds (Northern Apennine front, Italy). *Boll Soc Geol Ital* 125(1):59–65
- Tufano R, Fusco F, De Vita P (2016) Spatial modeling of ash-fall pyroclastic deposits for the assessment of rainfall thresholds triggering debris flows in the Sarno and Lattari mountains (Campania, southern Italy). *Rendiconti Online Società Geologica Italiana* 41:210–213
- Tufano R, Cesarano M, Fusco F, De Vita P (2019) Probabilistic approaches for assessing rainfall thresholds triggering shallow landslides. The study case of the peri-Vesuvian area (southern Italy). *Italian Journal of Engineering Geology and Environment Special* 1:105–110. <https://doi.org/10.4408/IJEGE.2019-01.S-17>

- Tufano R, Formetta G, Calcaterra D, De Vita P (2021) Hydrological control of soil thickness spatial variability on the initiation of rainfall-induced shallow landslides using a three-dimensional model. *Landslides* 18:3367–3380. <https://doi.org/10.1007/s10346-021-01681-x>
- United States Department of Agriculture (USDA) (2014) Keys to soil taxonomy, 12th ed. United States Department of Agriculture, Natural Resources Conservation Service, Government Printing Office, Washington, DC, USA, p 372
- Vallet A, Varron D, Bertrand C, Fabbri O, Mudry J (2016) A multi-dimensional statistical rainfall threshold for deep landslides based on groundwater recharge and support vector machines. *Nat Hazards* 84(2):821–849. <https://doi.org/10.1007/s11069-016-2453-3>
- van Genuchten MT (1980) A closed form equation for predicting the hydraulic conductivity of unsaturated soils. *Soil Sci Soc Am J* 44:892–898. <https://doi.org/10.2136/sssaj1980.03615995004400050002x>
- Vennari C, Gariano SL, Antronico L, Brunetti MT, Iovine G, Peruccacci S, Terranova O, Guzzetti F (2014) Rainfall thresholds for shallow landslide occurrence in Calabria, southern Italy. *Nat Hazard* 14:317–330. <https://doi.org/10.5194/nhess-14-317-2014>
- Vercesi PL, Scagni G (1984) Osservazioni sui depositi conglomeratici dello sperone collinare di Stradella. *Rend Soc Geol Ital* 7:23–26
- Vessia G, Parise M, Brunetti MT, Peruccacci S, Rossi M, Vennari C, Guzzetti F (2014) Automated reconstruction of rainfall events responsible for shallow landslides. *Nat Hazard* 14:2399–2408
- Vessia G, Di Curzio D, Chiaudani A, Rusi S (2020) Regional rainfall threshold maps drawn through multivariate geostatistical techniques for shallow landslide hazard zonation. *Sci Total Environ* 70525:135815
- Vitale S, Ciarcia S (2018) Tectono-stratigraphic setting of the Campania region (southern Italy). *J Maps* 14(2):9–21
- Watakabe T, Matsushi Y (2019) Lithological controls on hydrological processes that trigger shallow landslides: observations from granite and hornfels hillslopes in Hiroshima, Japan. *CATENA* 180:55–68. <https://doi.org/10.1016/j.catena.2019.04.010>
- Webb HR, Betacourt JL (1992) Climatic variability and flood frequency of the Santa Cruz River, Pima County, Arizona, US Geological Survey, 2379
- White ID, Mottershead DN, Harrison JJ (1992) Environmental systems: an introductory text, 2nd edn. Chapman & Hall, London, p 616
- Wieczorek GF, Morgan BA, Campbell RH (2000) Debris-flow hazards in the Blue Ridge of central Virginia. *Environ Eng Geosci* 6(1):3–23
- Wieczorek GF (1996) Landslide triggering mechanisms. In: Turner AK, Schuster RL (eds) Landslides: investigation and mitigation. Washington DC. Transportation Research Board, National Research Council, special report, pp 76–90
- Yune CY, Jun KJ, Kim KS, Kim GH, Lee SW (2010) Analysis of slope hazard-triggering rainfall characteristics in Gangwon Province by database construction. *J Korean Geotech Soc* 26(10):27–38
- Zizioli D, Meisina C, Valentino R, Montrasio L (2013) Comparison between different approaches to modelling shallow landslide susceptibility: a case history in Oltrepò Pavese, Northern Italy. *Nat Hazards Earth Syst Sci* 13:559–573. <https://doi.org/10.5194/nhess-13-559-2013>
- Zizioli D, Meisina C, Bordonni M, Zucca F (2014) Rainfall-triggered shallow landslides mapping through Pleiades images. In: Sassa K, Canuti P, Yin Y (eds) Landslide science for a safer geoenvironment. Springer, Cham, pp 325–329. [https://doi.org/10.1007/978-3-319-05050-8\\_51](https://doi.org/10.1007/978-3-319-05050-8_51)

**Publisher's Note** Springer Nature remains neutral with regard to jurisdictional claims in published maps and institutional affiliations.

## Authors and Affiliations

Francesco Fusco<sup>1,2</sup>  · Massimiliano Bordonni<sup>3</sup>  · Rita Tufano<sup>2</sup>  · Valerio Vivaldi<sup>3</sup>  ·  
Claudia Meisina<sup>3</sup>  · Roberto Valentino<sup>4</sup> · Marco Bittelli<sup>5</sup>  · Pantaleone De Vita<sup>2</sup> 

<sup>1</sup> Department of Civil and Environmental Engineering, Politecnico di Milano, Piazza Leonardo da Vinci, 32, 20133 Milan, Italy

<sup>2</sup> Department of Earth, Environmental and Resources Sciences (DiSTAR), University of Naples Federico II, Strada Vicinale Cupa Cintia, 21, 80126 Naples, Italy



- <sup>3</sup> Department of Earth and Environmental Sciences, University of Pavia, Via Ferrata, 1, 27100 Pavia, Italy
- <sup>4</sup> Department of Chemistry, Life Sciences and Environmental Sustainability, University of Parma, Parco Area delle Scienze, 157/A, 43124 Parma, Italy
- <sup>5</sup> Department of Agricultural Sciences, University of Bologna, Viale Fanin, 44, 40127 Bologna, Italy